Univerza *v Ljubljani*
Fakulteta *za farmacijo*

MARTIN GROSEK

MASTER'S THESIS

UNIFORM MASTER'S STUDY PROGRAMME PHARMACY

Ljubljana, 2017

UNIVERSITY OF LJUBLJANA
FACULTY OF PHARMACY

MARTIN GROSEK

ESTABLISHING ATG5 KNOCKOUT CELLS USING GENOME EDITING

VZPOSTAVITEV CELIČNEGA MODELA Z IZBITIM GENOM ATG5 Z METODOLOGIJO GENOMSKEGA PRIREJANJA

MASTER'S THESIS
UNIFORM MASTER'S STUDY PROGRAMME PHARMACY

Ljubljana, 2017

The present master thesis was realized at the Institute of Pharmacology at the University of Bern, with collaboration of the Faculty of Pharmacy, University of Ljubljana, under the mentorship of Prof. Dr. Irena Mlinarič Raščan and co-mentorship of Prof. Dr. Dr. Hans-Uwe Simon.

Acknowledgements

I would like to thank Prof. Dr. Dr. Hans-Uwe Simon for his guidance and for giving me the opportunity to work at his institute. I would also like to thank Prof. Dr. Irena Mlinarič Raščan for her mentorship. Special thanks goes to Dr. He Liu for her supervision of my work and other members of Prof. Simon Research group for their valuable contributions: Dr. Z. He, Nina, Živa, Flavia and Kevin. Great thanks also to Prof. Dr. Yousefi for her advice and to all the other members of PKI for creating welcoming and fruitful work environment.

Immense gratitude goes towards my parents and family who supported me on the path that has eventually led me to this work. Big thanks to my loving girlfriend Tea.

Finally, I will always greatly value all the friends who accompanied me during my days on the Faculty of pharmacy.

Statement

I hereby declare that I conducted my work to the best of my knowledge and carried out my master's thesis work independently under the mentorship of Prof. Dr. Irena Mlinarič Raščan and co-mentorship of Prof. Dr. Dr. Hans-Uwe Simon.

Ljubljana, 2017

President of the Thesis defence committee: Prof. Dr. Aleš Obreza
Member of the Thesis defence committee: Prof. Dr. Julijana Kristl

CONTENTS

TABLE OF FIGURES

TABLES

ABSTRACT

CRISPR/Cas9 technology is a novel genome-engineering tool that gained its popularity among scientific community due to its precise fast and efficient genome editing capabilities. We use it in this work for attaining gene knockout cell line, that will provide a platform for studying the effects of autophagy, and autophagy-related protein 5.

Autophagy is an evolutionary conserved intracellular process, responsible for sustaining cellular homeostasis under physiological and stressful conditions by controlled recycling and degradation of dysfunctional or abundant cell constituents within the lysosomes. Responsible for regulation of autophagy are autophagy-related (ATG) proteins. ATG5 is one of them and plays an essential role in autophagosome elongation and is thus indispensable for autophagic process. Autophagy can be, if defective or not properly regulated, involved in different contexts of pathophysiological pathways among others of cancerogenesis.

In our study, we used H1299, a commercially available human non-small cell lung cancer cell line and targeted *ATG5* genomic locus using CRISPR/Cas9 technology, producing H1299 *ATG5* knockout (KO) cells. We validated KO cells and confirmed a complete lack of ATG5 protein expression in cells targeted with one of the three CRISPR/Cas9 constructs. We noted that knockout of *ATG5* has disrupting effect on autophagy in H1299 *ATG5* KO cells by analyzing expression of several proteins involved in the autophagic process. We confirmed this, by inducing autophagy with starvation and simultaneous inhibition of degradation in lysosomes using chloroquine. Main methodologies were immunoblotting and fluorescent microscopy. Finally, we report increased growth rate of H1299 *ATG5* KO cells.

KEY WORDS: *Autophagy • ATG5 • ATG5 knockout • Cancer • CRISPR/Cas9*

RAZŠIRJENI POVZETEK

Avtofagija je znotrajcelični katabolični proces, ki omogoča razgradnjo citoplazemskih makromolekul v lizosomih. Vselej je prisotna na bazalnem nivoju v večini celic in tako skrbi za razgradnjo morebitnih napačno zvitih proteinov in okvarjenih organelov, njena aktivnost pa se lahko močno poviša v stresnih pogojih, kot so stradanje, oksidativni stres, pomanjkanje kisika. Takrat avtofagija z ragradnjo makromolekul celici omogoči gradnike za pridobivanje energije ali sintezo novih proteinov. Za mehanizem avtofagije so ključni z avtofagijo povezani (ATG) proteini, med njimi je ATG5, ki je nepogrešljiv pri nastajanju in dozorevanju avtofagosomov, za avtofagijo značilnih organelov preko katerih se materal za razgradnjo prenaša v lizosome. Avtofagija pa naj bi bila odgovorna tudi za programirano celično smrt, alternativno apoptozi. Za celično homeostazo je torej ključno natančno uravnavanje tega procesa, ki lahko, če je izkrivljen, privede do razvoja različnih patoloških stanj. Avtofagija je tako med drugim povezana z razvojem nevrodegenerativnih bolezni in malignih obolenj. Njena vloga pri tem pa je vse prej kot enoznačna, saj lahko v različnih okoliščinah pripomore k nastanku ali pa zavre razvoj bolezni.

CRISPR/Cas9 (angl. skupki enakomerno porazdeljenih kratkih palindromskih ponovitev/s CRISPR povezan protein 9) je orodje za prirejanje genoma, razvito na podlagi naravno prisotnega pridobljenega imunskega sistema nekaterih bakterij. Različice tega omogočajo bakterijam obrambo pred bakteriofagi, in sicer s shranjevanjem koščkov zaporedij zapisov napadalnega bakteriofaga ob prvem stiku. Zaporedja, shranjena v bakterijskem CRISPR lokusu, omogočajo prepoznavo bakteriofaga ob ponovnem kontaktu in služijo kot vodniška zaporedja za bakterijske endonukleaze. Cas endonukleaze, se lahko tako specifično vežejo in razrežejo genski zapis invazivnega bakteriofaga. Raziskovalci so izkoristili univerzalnost Cas9 endonukleaze iz *Streptococcus pyogenes*, ki jo je mogoče natančno voditi z 20 nukleotidnim vodniškim zaporedjem (guide RNA) in optimizirali model vodniškega zaporedja, tako je nastal prirejeni dvokomponentni sistem CRISPR/Cas9. Cas9 se na podlagi komplementarnosti baz vodniškega zaporedja veže na tarčno zaporedje, ki mora na 5’ koncu obvezno imeti za Cas9 specifično zaporedje PAM (NGG; poljubna nukleobaza in dva gvanina), ki je ključno za uspešno vezavo in aktivacijo Cas9, ki lahko tako prereže obe verigi tarčnega zaporedja 3~4 nukleotide za PAM. S spreminjanjem 20 nukleotidnega vodniškega zaporedja lahko tako izbiramo poljubno tarčo po principu

komplementarnosti, z omejitvijo, da mora ta tarča ležati neposredno ob PAM. Po dvoverižni prekinitvi DNA, se v tarčni celici aktivirata dva popravljalna mehanizma, in sicer visoko učinkovit, a nenatančen mehanizem nehomolognega združevanja prekinjenih koncev in natančen, vendar manj učinkovit mehanizem s homologijo vodenega popravljanja, ki potrebuje še predlogo zaporedja, po katerem mehanizem poteka. Prvi način je uporaben za izbijanje genov, saj mutacije povzročene po nenatančnem nehomolognem združevanju koncev, pogosto povzročijo nefunkcionalnost gena, drugi pa predvsem za vstavljanje novih genov.

Namen magistrske naloge je vzpostavitev celičnega modela iz komercialno dostopne humane celične linije nedrobnoceličnega pljučnega raka H1299 z izbitim genom ATG5 in ga validirati z vidika aktivnosti avtofagije in morebitnega vpliva na proliferativno sposobnost celic in vitro.

Izbitje gena ATG5

Z uporabo CRISPR/Cas9 tehnologije smo ciljali ekson 2 gena ATG5, in sicer smo s pomočjo spletno dostopnega orodja izbrali 3 najprimernejše vodniške RNA na podlagi njihove specifičnosti oz. verjetnosti njihovega ujemanja izven tarčnega zaporedja. Posamezno vodniško RNA smo nato vključili v komercialno dostopen plazmid LentiCRISPRv2, ki vsebuje mesto začetka podvojevanja, ki omogoča pomnoževanje vektorja v bakterijskih celicah, gen za antibiotično odpornost, ki omogoča selekcijo in ustrezne promotorje za izražanje v sesalskih celicah. Plazmide z vključeno vodniško RNA smo pomnožili v Stbl3 bakterijah, jih izolirali in sestavili v viruse z ovojničnim in pakirnim vektorjem. Nato smo pomnožili še viruse v HEK293T celicah in z njimi okužili H1299 celice. Celice, ki so uspešno izražale gen za rezistenco na puromicin, vstavljen v celico z virusom, smo izolirali. Del izoliranih celic smo obdržali v celični kulturi, del pa lizirali in analizirali njihovo izražanje proteinov s prenosom western. Ugotovili smo da je izmed treh vodniških RNA, samo ena povzročila uspešno izbitje gena ATG5, kar se je odražalo z odsotnostjo z avtofagijo povezanega proteina 5.

Za uspešno izolacijo celic z izraženim genom za rezistenco na puromicin, smo morali najprej določiti minimalno učinkovito koncentracijo puromicina, ki v tednu selekcijskega pritiska onemogoči preživetje celicam, ki ne izražajo tega gena. V ta namen smo enako

število celic izpostavili različnim koncentracijam puromicina in spremljali njihovo morfologijo ter število. Določili smo najnižjo učinkovito koncentracijo puromicina, in sicer 3 μg/ml.

Validacija celic z izbitim genom ATG5

H1299 celice z izbitim genom ATG5 smo primerjali s kontrolnimi celicami okuženimi z virusom, ki je vseboval enak plazmid vendar brez vodniške RNA. S prenosom western smo preverili izražanje proteinov, ki odražajo aktivnost avtofagije v celicah, in sicer poleg ATG5 še P62, LC3-I in LC3-II. Celice z izbitim *ATG5* pričakovano niso izražale proteina ATG5, hkrati pa so imele povišan nivo proteinov P62 in LC3-I ter znižan nivo proteina LC3-II v primerjavi s kontrolnimi celicami. Takšen rezultat kaže na nedelujoč oz. okrnjen proces avtofagije v celicah z izbitim *ATG5*. To smo potrdili z naslednjim poskusom pri katerem smo primerjali odziv celic inkubiranih 30 min v normalnih pogojih v rastnem mediju z in brez dodatka klorokina (CQ) ter v pogojih aminokislinskega stradanja v mediju EBSS z in brez dodatka CQ. Poleg določevanja izraženih proteinov ATG5, P62, LC3-I in LC3-II z imunoprecipitacijo in prenosom western, smo preverili izražanje ATG5 in LC3 tudi z imunofluorescenčnim označevanjem in fluorescenčno mikroskopijo.

Na koncu smo preverili še vpliv izbitja gena ATG5 iz H1299 celic na njihovo rast. V ta namen smo določili rastni krivulji H1299 kontrolnih celic in celic z izbitim *ATG5*. Vzporedno smo posadili enako število obeh celičnih tipov in 8 zaporednih dni prešteli njihovo število. Dobili smo rastni krivulji sigmoidne oblike, za kateri smo primerjali prileganje trem rastnim modelom, in sicer modelu logistične, Gompertzove in Weibullove rasti. Obe rastni krivulji sta najbolj ustrezali Weibullovemu modelu rasti. Potrdili smo tudi, da z ločenima krivuljama za H1299 kontrolne in celice z izbitim *ATG5* bolje opišemo njuno rast ter da imajo H1299 celice z izbitim *ATG5* signifikantno hitrejšo rast.

Naše delo predstavlja majhen prispevek k razkrivanju vloge avtofagije, oziroma ATG5 pri razvoju rakavih bolezni, z uporabo inovativnih pristopov, katerih nadaljnji razvoj bi omogočal hitrejše in enostavnejše doseganje tega cilja.

KLJUČNE BESEDE: *Avtofagija • Z avtofagijo povezan protein 5 (ATG5) • izbitje ATG5 • Rak • CRISPR/Cas9*

LIST OF ABBREVIATIONS

ATG	Autophagy related (gene)
ATG	Autophagy-related (protein)
BCA	Bicinchoninic acid
BP	Base pair
BSA	Bovine serum albumin
CAS	CRISPR associated
CQ	Chloroquine
CRISPR	Clustered regularly interspaced short palindromic repeats
crRNA	CRISPR RNA
DAPI	4',6-Diamidino-2-Phenylindole
dCAS9	Deactivated CRISPR-associated protein 9
DMSO	Dimethyl sulfoxide
DSB	Double stranded break
DTT	Dithiothreitol
EBSS	Earle's Balanced Salt Solution
ECL	Enhanced chemiluminescence
EDTA	Ethylenediamine tetraacetic acid
FCS	Fetal calf serum
GFP	Green fluorescent protein
HDR	Homology directed repair
HRP	Horseradish peroxidase
mTOR	Mechanistic target of rapamycin
NHEJ	Non-homologous end joining
NT	Nucleotide
PAM	Protospacer adjacent motif
PBS	Phosphate buffered saline
PFA	Paraformaldehyde
PI3K	Phosphoinositide 3-kinase
PMSF	Phenylmethanesulfonylfluoride
RT	Room temperature

SDS-PAGE	Sodium dodecyl sulfate polyacrylamide gel electrophoresis
sgRNA	Single guide RNA
TBS	Tris-buffered saline
TracrRNA	Trans-activating CRISPR RNA

1 INTRODUCTION

1.1 CRISPR/Cas – from bacterial immune system to genome engineering tool

Clustered regularly interspaced short palindromic repeats (CRISPRs) are sections of prokaryotic DNA consisting of short repetitive sequences (24-47 bases), which are divided by non-repetitive spacer sequences that match exogenous DNA (1-5).

The phenomena of CRISPRs was first observed in the genome of *Escherichia coli* back in 1987, when Ishino and colleagues stumbled upon peculiar set of evenly distributed 29-bp repeats which were interspaced by nonrepetitive sequences (6). Similar observations were made by other researchers in many other prokaryotes (7). Around 90% of sequenced genomes of arachea and half of that in bacteria have at least one CRISPR locus (8). Soon followed the identification of CRISPR associated (Cas) genes, located next to CRISPR sequences (9). But the function of CRISPRs remained unclear until the discovery that the origin of many spacer sequences within CRISPRs is of foreign genetic material, namely viruses and plasmids (10, 11) and that there is a correlation between the susceptibility of bacteria to certain phages and the absence of spacers in CRISPR loci of the same bacteria that match the sequence of the phage (the protospacer sequence) (10).

First undisputed evidence that type CRISPR/Cas system functions as bacterial adaptive immune system was provided in 2007, in experiment where *Streptoccocus thermophilus* had been infected with lytic phages, upon which bacteria incorporated new spacers that matched parts of DNA from newly encountered phages into their CRISPR region. This integration of spacers proved to be crucial for resistance from future infections from same phages (12). This discovery quickly came to practice, when they utilized the existing CRISPR/Cas system in cultured lactic acid bacteria, used in dairy industry, for obtaining strains of bacteria immune to some known harmful viruses that caused major problems in the industry (13). Soon thereafter the mechanism of CRISPR/Cas system began to unfold, as it was shown that after transcription of CRISPR loci, Cas proteins cut CRISPR RNA precursor in each repeat and mature CRISPR RNAs (crRNA) which contain virus derived sequences are used as small guide RNA that enable Cas protein to inhibit virus

proliferation (1) by directly targeting the invading DNA (14) or in some cases RNA (15). Further advances in understanding the mechanism were made by recognition of short sequences that are directly adjacent to protospacers and were found to be crucial for target recognition by guide RNA-Cas protein complex (10). These protospacer adjacent motifs (PAM) serve as recognition sites on targeted DNA and provide a mark on where Cas endonuclease should bind and cut the DNA. PAM are sequences that are absent in bacterial genome and are only present in invading phages, thus preventing self-destruction of CRISPR locus (4).

Three types (I, II and III) of CRISPR/Cas systems have been identified. Each system consists of specific cluster of Cas genes and CRISPR RNA (crRNA). Distinctive feature of type II CRISPR system that also makes it so useful for genomic engineering applications, is that instead of a large complex of Cas proteins required for crRNA-guided targeting and cleavage, as is the case in type I and III CRISPR systems, in type II there is only one Cas protein needed (2).

Around this time full potential for type II CRISPR/Cas system as a powerful genome engineering tool was revealed, as it was discovered that trans-activating crRNA (tracrRNA) confers maturation of crRNA and that the mature crRNA that is base paired to tracrRNA forms a dual RNA structure (tracrRNA:crRNA), which directs Cas9 to sequence-specific double stranded break (DSB) of targeted DNA (4). From this naturally occurring dual tracrRNA:crRNA, a single guide RNA (sgRNA) that has all the functions preserved, was artificially engineered (2, 4) and CRISPR/Cas9 genome engineering tool was born.

1.2 CRIPR/Cas9

Cas9 is a DNA nuclease, which is a part of type II CRISPR system in *Streptococcus pyogenes*. It is comprised of two nuclease domains, HNH and RuvC-like. The former is responsible for cleaving the target strand of DNA and the latter cleaves the non-target DNA strand, thus acting simultaneously they produce a DSB (2, 4, 5). Cas9 has a specific PAM (NGG; a random DNA-base, followed by two guanines), which must directly precede targeted sequence in order Cas9 to function (2, 5).

The term CRISPR/Cas9 will hereafter refer to genome engineering technology (not the naturally occurring bacterial immune system in *S. pyogenes*).

Although other genome engineering technologies that are based on engineered nucleases have been developed, such as zinc-finger nucleases (ZFNs) and transcription activator-like effector nucleases (TALENs), CRISPER/Cas9 holds some advantage over them. It has superior targeting efficacy, it can be leveraged for simultaneous modifications of several genes and is at the same time easier to use, less expensive and faster to customize (5).

CRISPR/Cas9 is a two-component system, composed of sgRNA and Cas9 (Figure 1). sgRNA has a 20-nucleotide guide sequence at the 5' end that determines the target site by base pairing and a scaffold sequence at the 3' end that binds to the Cas9. Specific binding of Cas9 nuclease to the target of interest only requires a complementary 20 nucleobase sequence as a guide sequence, the only limitation is that the target sequence has to be directly adjacent to PAM (5'NGG). Programing the CRISPR/Cas9 to target desired sequence is therefore only a matter of a change in the guide sequence of sgRNA. (2)

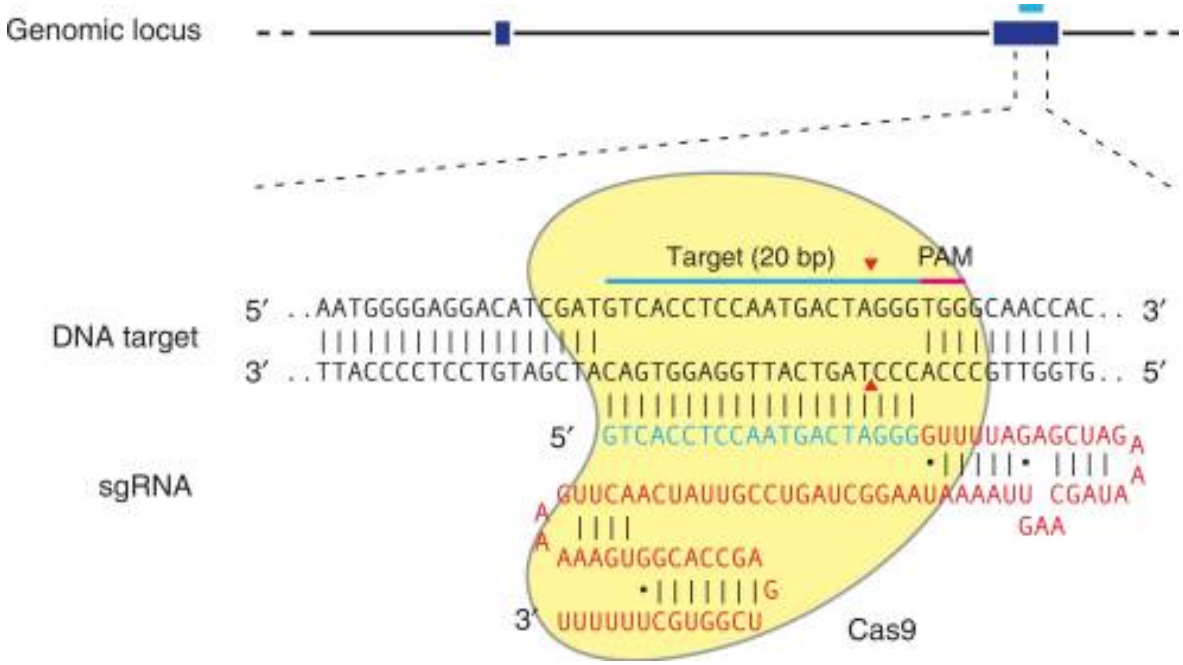

Figure 1: Depiction of Cas9 guided by sgRNA.

sgRNA consists of scaffold sequence (depicted in red), which binds to the Cas9 (in yellow), and 20-bp guide sequence (in blue), responsible for target recognition (blue bar) based on Watson-Crick base-pairing. Target DNA of 20-bp needs to be directly upstream of the PAM sequence of 5'NGG (pink bar). Cas9 cuts both strands of the target DNA 3 bp upstream of PAM, creating a DSB (red triangle). Nucleotide sequences in this figure, with exception of PAM, are symbolic and only serve as an example. (5)

Cas9 is precisely guided to its target by base pairing of the 20-nucleotide guide sequence to the target sequence directly upstream of PAM, but there are possible off-target effects due to off-target binding and cleavage. It was shown that up to 5-nucleotide mismatch between guide sequence and target sequence could still result in a successful binding of Cas9, although Cas9 rarely cleaves the DNA in such case. Efforts have been made to minimize potential off target effects with various algorithmic tools, capable of calculating possible off-target matches of the guide sequence, enabling the selection of the best-suited sequences, with least potential off-targets. (3) Approach to use longer guide sequences, up to 30-nt, for higher specificity, turned out to be unsuccessful because extended 5' end gets trimmed in vivo (16). Surprisingly truncated form of only 17-nt showed higher specificity (17). Target specificity increases also with the use of Cas9 nickase mutants (Cas9n), that have one of the two nuclease domains disabled, thus they only produce a single-strand break of the specific strand of the target DNA. When two such complementary mutants are used with their target appropriately selected, two single-strand breaks can actually result in a DSB, but with markedly increased specificity (16).

When Cas9 binds to the target and cleaves it, producing DSB in the DNA chain, two major repair mechanisms are usually activated, the Non-Homologous End Joining (NHEJ), which is error prone or Homology-Directed Repair (HDR), which requires a repair template. DSBs are re-joined by NHEJ if there is no homologue DNA piece as a repair template available, and because NHEJ is an error prone process, mutations occur in the form of insertion/deletion (indels). NHEJ can be utilized for inducing gene knockouts, because indels in the coding region can lead to frame shift mutations and subsequent premature stop codon (5).

On the other hand, HDR occurs at much lower rate and exclusively in dividing cells, but can be harnessed to produce specific DNA modifications in the presence of engineered repair template. The repair template can be a double-stranded DNA with homology arms flanking the defined cuts of targeted DNA or simply a single-stranded oligonucleotide (5, 18).

1.3 Use of CRISPR/Cas9 in research and clinical practice

CRISPR/Cas9 has been successfully used in various applications. It was used to recreate chromosomal translocations typical for tumors to establish human cell line models for studying consequences of genomic rearrangements for cancer development (19). It also greatly reduces time to generate transgenic animal models in comparison to the standard approach where the time consuming process involves generation of edited embryonic stem cell lines, injecting them into blastocyst embryos producing a chimeric animal that still need to produce offspring expressing desired mutation. On the other hand, injection of CRISPR system components into single-cell embryo can directly produce desired homozygotes (20).

The feature of CRISPR/Cas9 to be precisely guided to bind on a specific target DNA sequence was repurposed also for gene regulation. Catalytically deactivated Cas9 (dCas9) was developed, which can specifically bind to the target but cannot cut it (5). This enabled gene regulation on a genome-wide scale in a manner similar to RNA interference (RNAi), but unlike RNAi, which regulates gene expression on mRNA level and is mostly restricted to suppressing gene expression, dCas9 can also be tagged with a transcriptional activator and increase specific gene expression (2). DCas9 can also be exploited for imaging specific genomic loci in live cells when tagged with green fluorescence protein (GFP) (21), which is useful in studying conformational dynamics of native chromosomes (2).
The technology also provided an elegant and effective way for systematic analysis of gene functions using genome-scale gRNA libraries. Although RNAi is also used for this pooled loss-of-function genetic screening, CRISPR approach is more accurate with less off targets and more complete suppression of protein expression (22).

Human clinical trials using CRISPR technology are already underway, the first began in late October 2016 in China, where cancer patients received autologous ex vivo modified (with CRISPR/Cas) immune cells (23).
CRISPR/Cas9 technology has a potential to eradicate serious genetic disorders but there are ethical and safety issues regarding its use in editing human germline (2, 24). With current rapid advancements the field, it looks like ethical dilemmas pose the greater hurdle.

1.4 Introduction to autophagy

Autophagy is an evolutionary conserved, regulated intracellular catabolic process by which redundant or defective cell components are degraded in lysosomes in order to ensure survival and cellular homeostasis under stressful conditions (25-30). Although there are three major types of autophagy; macroautophagy, microautophagy and chaperone-mediated autophagy, macroautophagy is the most researched of the three (25, 30) and as the focus of this master thesis, it will be hereafter simply termed autophagy.

The onset of the active process of autophagy denotes formation of double-membrane vesicle termed autophagosome, which engulfs malfunctioning organelles, misfolded or simply excess proteins or other macromolecules. Autophagosome then fuses with lysosome, generating autophagolysosome in which sequestered cell constituents are degraded, providing cell with new components for energy production or future protein synthesis (25-30). As a dynamic process of cell components recycling, autophagy normally occurs at a basal level in most tissues, but it can be induced under unfavorable conditions (31). Autophagy may serve as a response mechanism of the cell, when the cell is exposed to growth factor or nutrient deprivation, reactive oxygen species, microbial pathogen infections or accumulation of defective proteins (27, 30). With advancing research in the field, the increasing complexity and importance of autophagy has been revealed, implicating its role in various physiological and pathological processes such as immunity, ageing, apoptosis, neurodegeneration and cancer (25, 27, 31-33). Having such pleiotropic effect, it is clear that autophagy needs to be tightly regulated and there is ongoing research on autophagy as a potential therapeutic target.

1.5 Molecular mechanisms of autophagy

Although autophagy was first discovered in mammals, foundations for understanding the molecular mechanisms of autophagy were made by discovering ATG genes in yeast, followed by their orthologs in mammals (25, 34). There are 19 known ATG proteins involved in mammalian autophagy (35). The whole process of autophagy can be divided into three major sequential steps: initiation, autophagosome formation and degradation of substrates.

The main player in the initiation step of autophagy is the mechanistic target of rapamycin complex 1 (mTORC1), which acts as a sensor for nutrient availability (26, 34, 36, 37). It also responds to (as the name suggests) rapamycin and other stimuli, such as growth factors, oxidative stress and mechanical stimuli (38). In nutrient abundant environment, mTORC1 is activated and as such maintains inhibitory phosphorylation on UNC-51-like kinases (Ulk1/2 - mammalian paralogues of yeast ATG1). Starvation on the other hand, triggers inactivation of mTORC1, which dissociates from Ulk1/2, allowing complex formation between Ulk1/2, ATG13 and scaffold protein FIP200 (orthologue of yeast ATG17). Accumulation of this complex at the isolation membrane named phagophore marks the start of autophagosome formation (34, 36, 39). Localization of another protein complex, containing a class III phosphatidylinositol 3-kinase (PI3K), ATG14 ligand and beclin 1 (mammalian orthologue of ATG6), facilitates the local production of phosphatidylinositol 3-phosphate (PI3P), which recruits other ATG proteins such as ATG9, necessary for the expansion of the phagophore (26, 34, 39).

Two ubiquitin-like conjugation systems are responsible for expansion and elongation of the phagophore membrane. In the first, ATG12 is conjugated to ATG5 in a process facilitated by E1 and E2-like enzymes, ATG7 and ATG10, respectively. ATG12-ATG5 conjugate then interacts with ATG16L, forming complex, which self-oligomerizes into a tetramer (37). The second is the microtubule-associated light chain 3 phosphatidylethanolamine (LC3-PE) conjugation system. LC3 (mammalian paralogue of yeast ATG8) is first cleaved by ATG4, generating the cytosolic LC3-I. Following conjugation of LC3-I to PE requires ATG7 (E1-like enzyme) and ATG3 (E2-like enzyme). LC3-PE or LC3-II is attached to the autophagosome membrane (26, 36, 39, 40).

In the final stage, the mature autophagosome fuses with lysosome, forming autolysosome (also called autophagolysosome), the process mediated by syntaxin 17, a member of SNARE protein family. In the acidic environment of autolysosomes, degradation of the cargo occurs by the on-site hydrolases and lipases (26, 28, 34).

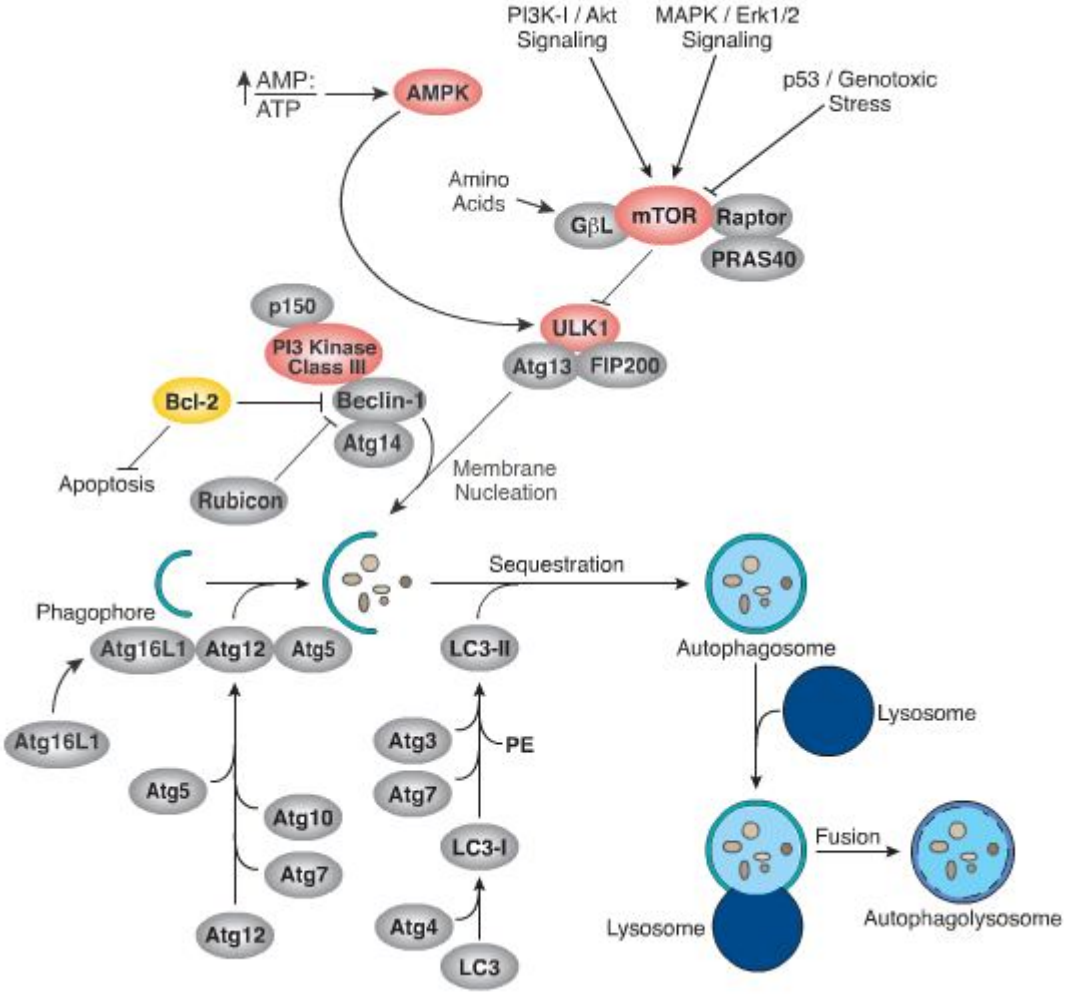

Figure 2: Schematic presentation of autophagy pathway and its core molecular machinery.

Four major protein complexes compose autophagic machinery: ULK1 complex, class III PI3K complex and two ubiquitin-like conjugation systems ATG12-ATG5 and LC3-PE. UNC-51-like kinase 1 (ULK1) (a mammalian paralogue of yeast ATG1) represents a critical point for autophagy initiation. Upstream regulators of ULK1 are the mTOR Complex 1 (mTORC1) and AMP activated protein kinase (AMPK). The mTORC1, consisting of mTOR, G-protein β subunit-like (GβL), proline-rich AKT1 substrate (PRAS40) and regulatory associated protein of mTOR (RAPTOR), has a function of nutrient/redox/energy sensor. In nutrient abundant environment, mTORC1 is activated and as such maintains inhibitory phosphorylation on ULK1. Unfavorable conditions (nutrient deprivation, oxidative stress) on the other hand, trigger inactivation of mTORC1, which dissociates from ULK, allowing complex formation between ULK1, ATG13 and the scaffold protein FIP200 (mammalian orthologue of yest ATG17), which enables the start of autophagosome formation. Energy depletion can also trigger autophagy through direct activation of ULK1 by AMPK.
Class III PI3K complex, consisting of beclin 1 (ATG6), hVps34 (class III PI3 kinase), Atg14-like protein (Atg14L) and serine/threonine kinase p150, regulates nucleation of autophagosomal membrane. B-cell lymphoma-2 (Bcl-2), an antiapoptotic protein, regulates function of beclin 1 in autophagy by binding and sequestering beclin 1 under nutrient abundant conditions and so the dissociation of beclin 1 from Bcl-2 is required for autophagy induction (41). This PI3K complex further recruits ATG12-ATG5 and LC3-PE ubiquitin-like conjugation systems, which are involved in the autophagosome elongation and maturation. Autophagosome with enclosed cargo then fuses with lysosome, forming autophagolysosome, where the cargo gets degraded. (34)
Illustration reproduced courtesy of Cell Signaling Technology, Inc. (www.cellsignal.com)

1.6 Autophagy and cancer

Autophagy has a conflicting role in cancer. In different contexts, it can be involved in tumor suppression and tumor progression. Its role in early stages of tumor formation is believed to be mainly protective, whereas in established tumors it may act in favor of tumor survival, progression and in some cases even cause resistance of malignant cells to anticancer therapy (26, 27, 29, 32).

Experiments in animal models with defective autophagy achieved by tissue specific or whole body knockouts of crucial ATG genes showed increased spontaneous occurrence of tumors as well as their accelerated development (29). Murine model of heterozygous knockout of *BECN 1* (encoding for beclin 1, a mammalian orthologue of ATG6) spontaneously develops a number of malignant transformations from liver and lung carcinoma to lymphomas (29). Furthermore, monoallelic deletions of *BECN 1* have been found in many samples of breast, ovarian and prostate cancers in human (42). On similar note, mosaic deletion (only in liver, heart, brain and skeletal muscle) of *ATG5* in mice (complete knockout of *ATG5* is neonataly lethal (43)) resulted in spontaneous occurrence of hepatic tumors (44). In support of tumor suppressive role of autophagy are also findings from a research where significantly decreased levels of ATG5 were found in patients suffering from primary melanoma as compared to those with benign nevi. Melanoma patients with higher ATG5 levels also had better progression free survival as opposed to those with lower ATG5 levels (45).

All these findings suggest protective role of autophagy against tumor development and several mechanisms have been proposed. Autophagy may act as tumor suppressor by promoting oncogene-induced senescence and thus preventing proliferation of transformed cells (45). Down-regulation of ATG5 in melanocytes was shown to diminish basal level of autophagy, increase cell proliferation and at the same time absence of oncogene-induced senescence was observed (45). Another tumor suppressive mechanism could be the suppression of inflammatory response caused by necrosis. Necrosis is a common feature in solid tumors and is associated with poor prognosis. Disruption of autophagy in apoptosis-deficient tumors promotes necrosis and affiliated inflammation, resulting in accelerated tumor growth (46).

Basal levels of autophagy provide the cell with an effective way to get rid of defective cell constituents and to contribute to cell homeostasis. Insufficient levels of autophagy can thus lead to the accumulation of damaged cell organelles and macromolecules that can result in increased oxidative stress, unstable genome and DNA damage that can give rise to oncogenic mutations (27, 47, 48). One such example is accumulation of P62 protein, which is a substrate for autophagy degradation. In autophagy deficient tumors, accumulation of P62 was shown to enhance tumor growth and P62 elimination counteracted this effect (48).

While autophagy may have protective role in the early stages of cancerogenesis, preventing tumor formation, tables can turn when transformed cells slip the crack of anticancer defense and then autophagy could work in favor of malignant cell survival and enable tumor progression (29). Malignant cells are subjected to various intra- and extracellular stressful stimuli, especially when they gain metastatic properties. In these settings, autophagy is proposed to compensate for increased oxidative stress, hypoxic environment and nutrient deprivation due to higher nutrient demand, enabling cell survival (49). Indeed advanced stage tumors were often found to have increased autophagic flux, which correlated with the metastatic phenotype and poor prognosis (29).

Anticancer therapeutics often evoke stressful stimuli in tumor microenvironment that induce autophagy. Conventional cytotoxic drugs as well as radiation therapy were shown to induce autophagy (50). Other newer agents also include gefitinib and erlotinib (51), imatinib (52), cetuximab (53), vorinostat (54). But autophagic responses may act as a buffer, desensitizing tumor cells to intra- and extracellular stressful stimuli in tumor microenvironment and contribute to increased resistance to anti-cancer therapy (27, 29). All this data suggest that inhibiting autophagy in certain cases could be a suitable therapeutic approach in cancer therapy. Promising results have been reported in studies investigating concomitant treatment of cancer cell lines with anti-cancer agents and autophagy inhibition achieved either by pharmacological inhibitors or genetic silencing of autophagy regulatory genes (55).

1.7 Methods for autophagy detection

Several approaches for measuring and detecting autophagy have been established. The

most straightforward method is the morphological detection of autophagosomes by electron microscopy. While this method is well established, it is rather inaccessible and expensive (56). More recent methods are based LC3, a mammalian paralogue of ATG8. LC3 is cleaved by ATG4, producing LC3-I, which is then conjugated to phosphatidylethanolamine (PE) to form LC3-II (34, 40). This lipidated form of LC3 is located on the inner and outer membranes of autophagosomes and can thus serve as a specific marker for their detection (37, 57). Expression of green fluorescent protein GFP-LC3 conjugates (N-terminal fusion of GFP to LC3 (58)) can be detected with fluorescent microscopy where GFP-positive structures correspond to autophagosomes (59). Indirect immunofluorescence approach can be used as well, with specific antibodies conjugated with a fluorophore. Levels of LC3-I and LC3-II can serve as indicator of autophagic activity, based on conversion of LC3-I to LC3-II (37). In Western blot detection, bands of LC3-I and LC3-II are separated with SDS-PAGE, where LC3-II band is migrating faster due to its relative hydrophobic nature compared to LC3-I. (60)

Although detecting the number of autophagosomes by electron microscopy or LC3-II based assays described above give a good insight on the autophagic activity, it is not a reliable indicator of the actual situation. Namely because the number of autophagosomes itself does not explain whether the increase in the number of autophagosomes is a consequence of actual increased level of autophagy or an inhibition of autophagic process further downstream (37). For a better estimation of the actual autophagic activity, evaluation of autophagic flux, which refers to a complete autophagy process, from autophagosome formation, to conveyance of the substrates to lysosomes and their subsequent degradation, is needed (56). This can be achieved with the manipulation of autophagy with controlled induction and inhibition of autophagy. Autophagy induction in experimental settings is usually attained by starvation or rapamycin (inhibiting mTOR) and is inhibited with the use of inhibitors of the late stages of autophagy, such as cloroquine (CQ) or bafilomycin A1 (57). Both pharmacological agents cause rise of pH in acidic lysosomes and thus inhibit lysosomal enzymes and prevent fusion with autophagosomes (although the mechanisms by which this is achieved are not identical) (27). With intact autophagic machinery, specific inhibition of a late stage in autophagy causes a traffic jam-like effect, where intermediates up to a point of inhibited step buildup, this effect is even more prominent if the autophagy is induced at the same time. Inducing autophagy with

starvation or with pharmacological inducer such as rapamycin with and without of simultaneous use of before-mentioned inhibitors of the late stage of autophagy and then comparing the outcome with non-induced control, gives a better understanding of the actual autophagic activity (37, 39, 57).

Another useful marker for studying autophagic flux is p62 protein, which specifically binds to LC3 and is subsequently incorporated into autophagosomes, where it gets degraded. Because P62 is a specific substrate for autophagy degradation, levels of p62 decrease when autophagy is induced and conversely, accumulation of p62 occurs when autophagy is inhibited (57, 61).

Autophagy is a complex process, exerting several functions and is at the same time regulated by diverse mechanisms so drawing quick conclusions, based on results obtained with one method can be misleading. Because there is no single standard assay for accurate measurement of autophagic activity at the moment, use of multiple methods and careful evaluation of the results obtained is advised (57).

1.8 Autophagy-related protein 5

ATG5 protein is one of the essential components of autophagic machinery. Series of experiments regulating its expression have been conducted. In mice, the genome wide knockout of *ATG5* proved to be neonatally lethal (43).
A mutation of ATG5 was described in two human patients, who had decreased autophagy congenital ataxia and developmental delay (62).

Altering ATG5 expression either by RNAi or knockout models was often used to study functions of autophagy. Apart from its role in autophagy, ATG5 was shown to serve as a linkage between autophagy and apoptosis (Figure 3).

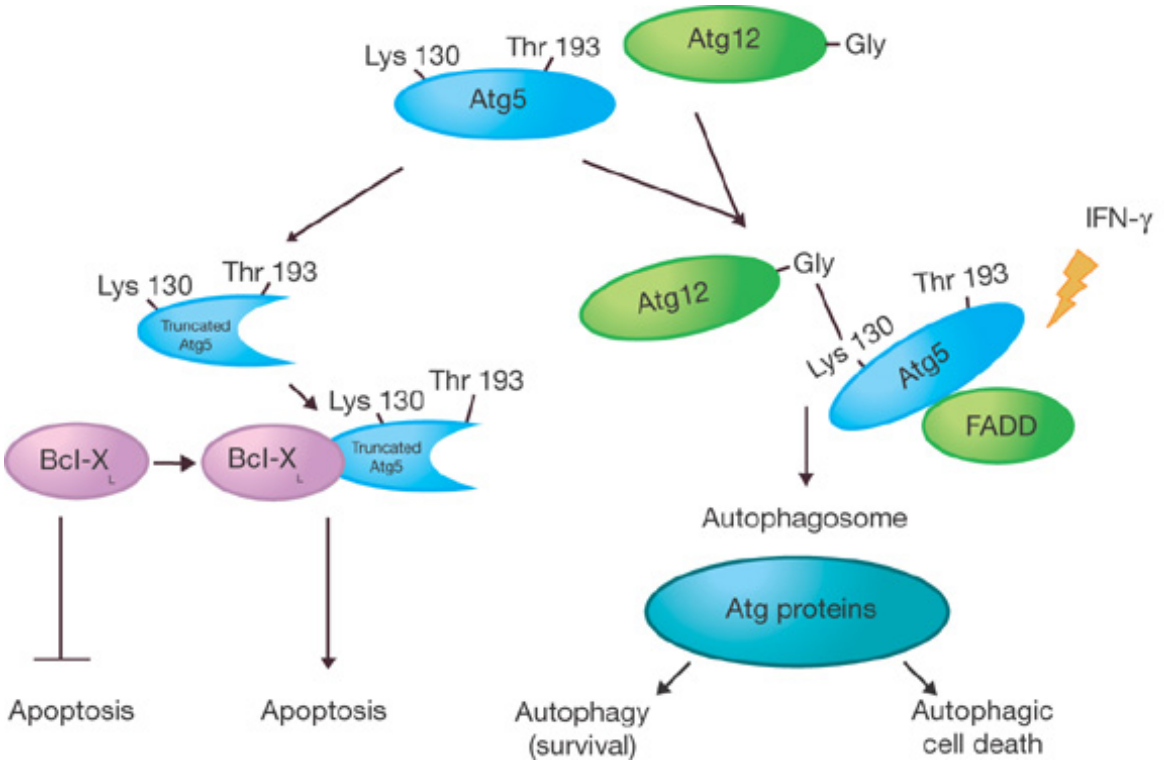

Figure 3: ATG5 function in autophagic cell death and crosstalk with apoptosis.

E1 and E2-like ubiquitin enzymes, ATG7 and ATG10 respectively, are necessary for ATG12 conjugation to ATG5, forming an isopeptide bond between lysin residue at position 130 in ATG5 and glycine residue in ATG12. ATG12-ATG5 conjugate plays an essential role in autophagosome formation and maturation. Autophagy is usually associated with cytoprotective role, maintaining cellular homeostasis at basal levels by degrading malfunctioning organelles and compensating nutrient deprivation by recycling cell constituents at induced levels. But the autophagic machinery can be in some circumstances also utilized in autophagic cell death, for example ATG5-ATG12 conjugate in response to interferon-γ (IFN-γ) stimulus, interacts with Fas-associated protein with Death Domain (FADD) to trigger autophagic cell death.

Unconjugated ATG5, although barely detectable in its free form, is also a substrate for calpain cleavage, producing the truncated form of ATG5 at position threonine 193. This truncated form of ATG5 is a pro-apoptotic molecule that translocates to mitochondria and likely asserts its pro-apoptotic function via binding to Bcl-$_{XL,}$ inactivating it and thus preventing the usual inactivation of Bax (a pro-apoptotic protein) by Bcl-$_{XL}$ (63, 64).

2 RESEARCH AIM

The aim of this thesis is to establish a H1299 cell line with *ATG5* gene knockout in order to further investigate its role in cancer. The *ATG5* gene encodes for ATG5 protein, an essential component of autophagic machinery, which runs the process of autophagy. Autophagy was shown to play part in pathophysiology of several diseases including cancer and is thus being considered as a potential therapeutic target. In this master thesis, we will use H1299, a commercially available human non-small cell lung carcinoma cell line, derived from a lymph node metastasis.

With CRISPR/Cas9 technology, using 3 different guide RNAs, we will target *ATG5* genomic locus of H1299 cell line in order to obtain cells lacking ATG5 protein expression. We will identify potential successful knockouts and further evaluate them, determining the effect of the genome modification on their autophagic activity and their growth rate. Methods used will include immunoblotting and immunofluorescent staining.

3 MATERIALS AND METHODS

3.1 Materials

Table I: Laboratory equipment

Name	Type	Company
Aspirating pipette	2 mL	Greiner Bio-One
Autoradiography film	Amersham Hyperfilm ECL	GE Healthcare
Cell culture flasks	TC Flasks with filter cap (50 mL, 250 mL, 550 mL)	Greiner Bio-One
Cell culture plates	6-, 24- and 96-well plates	Greiner Bio-One
Centrifuge	Heraeus Multifuge 3SR	Thermo Fisher Scientific
Confocal microscope	Zeiss observer Z1 LSM 700	Carl Zeiss
Counting chamber	Neubauer Improved	Assistent
Cryogenic vial	Nunc CryoTubes; 1.8 mL	Sigma
Cytoslides	Shandon Single Cytoslides	Thermo Scientific
Electronic analytical balance	XP205	Mettler Toledo
Electrophoresis machine	Powerpac 3000	BioRad
Electrophoresis System	XCell SureLoc Mini-Cell	Life Technologies
Falcon tubes	PP tubes with screw cap; 15 mL, 50 mL	Greiner Bio-One
Freezer (-20°C)	G 3513	Liebherr
Freezer (-80°C)	MDF-5386SC	Sanyo
Hybridisation Incubator	Hybridiser HB-1D	Techne

Imaging System	X-Omat 2000 processor	Kodak
Incubator	Heraeus HERAcell 150i	Thermo Fisher Scientific
Light microscope (inverted)	Zeiss Axiovert 35	Carl Zeiss
Magnetic stirrer	IKAMAG REO	Drehzal-electronics
Micro Test Tube	3810X; 1.5 mL	Eppendorf
Microcentrifuge	Centrifuge 5417 D	Eppendorf
Microcentrifuge	Centrifuge 5417 R	Eppendorf
Microplate reader	SpectraMax M2	Molecular Devices
Orbital shaker	GFL 3005	Faust
Pipette boy	Pipetboy acu	INTEGRA Biosciences
Pipettes	2.5 µL, 10 µL, 100 µL, 1000 µL	Eppendorf
Serological pipettes	5 mL, 10 mL, 25 mL	Eppendorf
Superspeed centrifuge	RC 5C PLUS	Sorvall
Thermomixer	Thermomixer compact	Eppendorf
Transfer membrane	Immobilon - P	EMD Millipore
Transfer membrane	Immobilon - FL	EMD Millipore
Vortex mixer	Vortex-Genie 2	Scientific Industries

Table II: Media and chemicals

Media and chemicals	Company
Chloroquine	Sigma
DMEM + GlutaMAX (Dulbecco's Modified Eagle Medium)	Invitrogen, Life Technologies
DMSO sterile	Sigma
DTT	Sigma
EBSS	Thermo Fisher Scientific
ECL Donkey anti rabbit IgG, HRP-linked antibody	GE Healthcare
ECL Sheep anti mouse IgG, HRP-linked antibody	GE Healthcare
FCS	PAA Laboratories
Goat-anti-mouse Antibody, 488	Invitrogen, Molecular Probes
Goat-anti-mouse Antibody, 555	Invitrogen, Molecular Probes
Goat-anti-rabbit Antibody, 488	Invitrogen, Molecular Probes
Goat-anti-rabbit Antibody, 568	Invitrogen, Molecular Probes
HEPES	Sigma
Mouse ATG5 Antibody (11C3)	NanoTools
Mouse ATG5 Antibody (7C6)	NanoTools
Mouse GAPDH Antibody	EMD Millipore
Mouse LC3 Antibody	NanoTools
Mouse p62 Antibody	Santa Cruz Biotechnology
NucleoBond Xtra Midi	MACHEREY-NAGEL
NuPAGE LDS Sample Buffer (4X)	Thermo Fisher Scientific
Paraformaldehyde	Sigma
PBS	PAA Laboratories
Penicillin-Streptomycin	Invitrogen, Life Technologies
Pierce BCA Protein Assay Kit	Thermo Fisher Scientific
Pierce ECL Plus Western Blotting Substrate	Thermo Fisher Scientific
Polybrene	Sigma

Pre-Stained Protein Standard Novex Sharp	Thermo Fisher Scientific
ProLong Gold Antifade Reagent with DAPI	Thermo Fisher Scientific
Protease inhibitor cocktail (104 mM AEBSF, 80 μM Aprotinin, 4 mM Bestatin, 1.4 mM E-64, 2 mM Leupeptin, 1.5mM Pepstatin A)	Sigma
Puromycin	InvivoGen
QIAquick Gel Extraction Kit	QIAGEN
Rabbit LC3 Antibody	Cell Signaling Technology
Restore Western Blot Stripping Buffer	Thermo Fisher Scientific
RPMI Medium 1640 + GlutaMAX	Invitrogen, Life Technologies
RunBlue 12% SDS PAGE Precast Gel	Expedeon
RunBlue SDS Running Buffer (20X)	Expedeon
Saponin	Sigma
Thermo Scientific FastDigest Esp3I	Thermo Fisher Scientific
Trypsin-EDTA	Thermo Fisher Scientific
Zyppy™ Plasmid Miniprep Kit	ZYMO RESEARCH
Borax anhydrous	Sigma
Sodium dihydrogen phosphate monohidrate	Merck Millipore

Table III: Prepared solutions

Prepared solution	Components
Blocking buffer for Western blot	5% milk powder in TBST
Blocking solution for immunofluorescence staining	3% goat serum and 0.05% saponin in PBS
Lysis buffer	50 mM Tris [pH 7.4], 150 mM NaCl, 10% Glycerol, 1% Triton X-100, 2 mM EDTA, 10 mM NaPyrophosphate, 50 mM NaF, 200 µM Na3VO4
TBS (10X)	0.20 M Tris, 1.50 M NaCl [pH 7.6]
TBST	0.1% Tween20 in TBS
Transfer buffer (10X)	0.25 M Tris, 1.87 M Glycine
Transfer buffer	20% MeOH in 1X Transfer buffer
Lab-made ECL working solution	5 mL buffer pH 9,5 (50 mM NaH_2PO4, 50 mM Na_2CO_3, 150 mM NaCl, 10 mM $Na_2O_7B_4$), 11 µM Coumaric acid, 25 µM Luminol, 1,5 uL 30% H_2O_2

3.2 Methods

3.2.1 Cell culture

a) Cell passaging

Passaging involves splitting cells and transferring a small number of cells into new culture flasks. Ideally this is done when cells are in the log phase of growth, that is when they are 10-90% confluent.

Cells were grown in culture flasks or dishes with the optimal culture media (Table IV), containing 10% FCS and 1% P/S (10 000 units/mL of penicillin and 10 000 µg/mL of streptomycin) at 37°C with 5% CO_2.

Adherent cells first need to be detached with trypsin-EDTA. A fraction of detached cells can then be used to expand a new culture, while the rest is discarded.

Before detachment, floating dead cells and any traces of serum that would hinder the dissociative action of trypsin are removed. This is achieved by removing the culture media from the flask by vacuum pump and washing with PBS. Then 0.5 mL (for small flask) / 1 mL (for middle flask) / 2 mL (for big flask) of trypsin-EDTA is added to the flask, which is then incubated for up to 5 min at 37°C to get the cells detached from the flask surface.

To resuspend cells, 4.5 mL (for small flask) / 9 mL (for middle flask) / 18 mL (for big flask) of complete fresh growth medium is added to the flask with detached cells. Cells are homogenized by pipetting up and down and transferred to a falcon tube, which is then spun in a centrifuge for 5 min at 1400 rpm. Cell pellet is resuspended in 1 mL of complete fresh growth medium and cells are counted as described in section d). An appropriate number of cells are then transferred to new pre-labeled flasks, already filled with fresh media pre-warmed to 37ºC. The new flasks are incubated for further cell propagation.

Table IV: Cell lines and corresponding optimal cell culture medium.

Cell line	Cell culture medium
H1299	RPMI + 10% FCS, 1% P/S
HEK293T	DMEM + 10% FCS, 1% P/S

b) Cell freezing

Cells are detached from the culture flask following the procedure for cell passaging. Resuspended cells are transferred to a 15 mL falcon tube. They are centrifuged at 1400 rpm for 5 min. After centrifugation the supernatant is carefully removed without disturbing the cell pellet. Cell pellet is resuspended in 1 mL of pre-cooled, freshly prepared 10% mixture of DMSO in FCS and transferred to the pre-labeled cryovial. The tube is closed and placed in a chamber containing isopropanol and stored at -80°C overnight. Later, vials are transferred to liquid nitrogen tank for indefinite storage.

c) Cell thawing

Vials containing frozen cells are removed from liquid nitrogen tank and put in 37°C water bath to allow rapid thawing of the cells. Meanwhile, 9 mL of pre-warmed growth medium is added to a 15 mL falcon tube. Then cells from the vial are gradually diluted with this medium and transferred to the falcon tube. The cells are shortly mixed with the pipette and then centrifuged at 1400 rpm for 5 min at RT. After centrifugation supernatant is removed. One milliliter of fresh media is added to the cell pellet, which is resuspended by pipetting. Then all the cells are transferred to the new pre-labeled flask, filled with fresh media. The flask is incubated at 37°C with 5% CO_2 for further culture.

d) Cell counting

Cells were detached from the culture flask/plate following the procedure for cell passaging. Neubauer chamber was prepared by placing a coverslip in the middle of that chamber. 10 ul of the homogeneous cell suspension, resuspended in a fixed volume of PBS, were transferred to the edge of the Neubauer counting chamber. A droplet of the cell suspension is expelled and drawn under the coverslip by capillary action. The chamber was placed under microscope and cells were counted in all 4 quadrants, each comprised of 16 squares. Cells overlapping the top and left borders of the quadrant were included in the counting but not those overlapping the bottom or right lines.

Concentration of cells was determined by the following calculation:

$$\text{Cells/mL} = (\text{number of cells counted} / 4) \times \text{dilution factor} \times 10^4$$

3.3 Puromycin titration

For determining the optimal concentration of puromycin needed for antibiotic selection of H1299 cells, a cell death curve was established by seeding 10'000 wild-type H1299 cells per well in a 24-well plate. The next day complete growth medium was replaced with dilutions of puromycin in complete growth medium with the concentration gradient from 8 to 0 μg/mL (Table V). Same concentration was used in duplicates. Cell culture plate was then incubated at 37^0C and 5% CO_2 and was daily inspected under the light microscope to observe potential visual toxic effects for up to 8 days. Fresh selective medium was replaced three times during this period. After 2, 4 and 8 days of incubation, pictures of cells were taken with Zeiss axiovert 35 microscope. After 4 days, a well per each puromycin concentration was washed, cells harvested (as described in 3.2.1a)), stained with 0.4% solution of trypan blue and viable cells were counted (as described in 3.2.1d)). The procedure was repeated with the remaining set of wells, after the cells had been under selection pressure of puromycin for 8 days in total.

Table V: Scheme of 24-well plate seeded with wild-type H1299 and concentrations of puromycin [μg/ml] used.

8	8	6	6	5	5
4	4	3,5	3,5	3	3
2,5	2,5	2	2	1,5	1,5
1	1	0,5	0,5	0	0

3.4 CRISPR/Cas9-mediated *ATG5* knockout

The *ATG5* genomic locus was targeted using the CRISPR/Cas9 technology producing H1299 cell lines devoid of ATG5 protein expression.

a) Transfer vector modifications

The lentiCRISPRv2 plasmid was a gift from Feng Zhang (Addgene plasmid #52961) (Sanjana et al. 2014) (Figure 4).

We designed 3 guide RNAs (gRNA1, gRNA2, gRNA3) targeting the exon 2 of human *ATG5* using the publicly available CRISPR design tool at http://crispr.mit.edu (65). After entering a DNA sequence of targeted gene and selecting the target genome, CRISPR

design tool scans the sequence for possible CRISPR guides and possible off-target matches throughout the selected genome. Then each potential guide sequence is automatically assigned a score up to a 100 based on their off target hit score (computed 100% minus a weighted sum of off-target hit-scores in the targeted genome, which is calculated based on an algorithm (3)). We selected the three highest scoring guide RNAs, with the least potential exon off-targets.

For initial plasmid purification NucleoBond Xtra midi kit from MACHEREY-NAGEL was used, following manufacturers instructions**.**

The next steps were taken according to the protocol (66), in summary; the plasmid was dephosphorylated, digested with FastDigest Esp3I (slight modification of the original protocol) and then separated with SDS-PAGE. Linearized plasmid was extracted using QIAquick Gel Extraction Kit. Later, primers (gRNAs) were annealed and ligated into the plasmid.

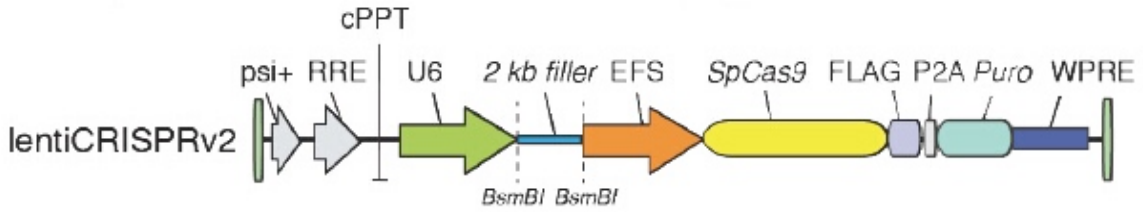

Figure 4: Schematic presentation of lentiCRISPRv2 and its vital components.

LentiCRISPRv2 sequence is composed of 14873 base pairs. psi; RNA target site for nucleocapsid packaging. RRE; (Rev Response Element) sequence to which the Rev protein binds. cPPT; (Central polypurine tract) recognition site for proviral DNA synthesis. U6 and EFS; human promoters. BsmBI: restriction enzyme cutting site. SpCas9; (*Streptococcus pyogenes* Cas9). FLAG; protein tag for mammalian expression. P2A;2A peptide that enables translation of multiple genes from the single transcript. Puro; puromycin resistance. WPRE; (Woodchuck hepatitis virus post-transcriptional regulatory element) sequence that stimulates the expression of transgenes via increased nuclear export. (67)

b) Bacterial transformation

To reproduce desired plasmids, competent Stbl3 bacteria were transformed. Bacteria were taken from the -80°C storage and thawed on ice. 50 ng of desired plasmid (one of the plasmids with gRNA1, gRNA2, gRNA3 inserts targeting human *ATG5* or control plasmid without the insert) were added to 100 ul of thawed bacteria, homogenization was done only by gentle swirling of the tubes, which were then put on heating block for 90 seconds at 42°C. After the heat shock, bacteria were incubated on ice for 30 min, followed by addition of 900 ul of LB (without antibiotics) and 45 min incubation on a shaker with 200

rpm at 37°C. 20 ul of mixture were then spread on pre-warmed selective (50 µg/mL carbenicillin) agar plates and incubated upside down at 37°C overnight. The next day, 4 single colonies per transformation were picked and transferred into 2 mL of LB medium (with 50 µg/mL carbenicillin) and incubated for 6 hours at 37°C, 200 rpm. To assure the presence of the inserts in the plasmids, screening PCR was performed. Specific gRNA reverse primers were used (Table VI) and hU6 (5'-GAGGGCCTATTTCCCATGATT-3') as forward primer. Clones 3 and 4 from each transformation were further grown overnight in LB at 37°C, 200 rpm. At this point, glycerol stocks of modified bacteria (clones 3 and 4) were made and stored at -80°C for further use. Plasmids were then purified using Zyppy™ Plasmid Miniprep Kit and plasmids from bacterial clones 4 were sent for sequencing at Microsynth Company to confirm the correct sequences.

Table VI: List of primers

Oligo Name	Sequence 5' to 3' (including restriction sites)
gRNA1forward	CACCGAACTTGTTTCACGCTATATC
gRNA1reverse	AAACGATATAGCGTGAAACAAGTTC
gRNA2forward	CACCGTGATATAGCGTGAAACAAGT
gRNA2reverse	AAACACTTGTTTCACGCTATATCAC
gRNA3forward	CACCGGTGCTTCGAGATGTGTGGTT
gRNA3reverse	AAACAACCACACATCTCGAAGCACC

c) Lentivirus production

HEK293T cells were seeded in a 6-well plate in DMEM with 10% FCS and antibiotics. 1.5 µg of modified plasmid (Table VII), 1 µg of envelope vector pMD2GVSV-G, 2.5 µg of packaging vector psPAX2 and 10 µL of X-tremeGENE HP DNA Transfection Reagent from Roche were gently mixed together and incubated for 20 min at RT. HEK293T cells were transfected by adding the individual mixture drop wise in the correspondent well. Plate was then incubated overnight at 37°C and 5% CO_2. Following day the medium was changed and supplemented with 10 mM HEPES. Viruses were harvested after 24h incubation by collecting the supernatant and were filter-sterilized.

Table VII: List of vectors

Plasmid (plasmid type_guide RNA_targeted gene)
LentiCRISPRv2_gRNA1_hATG5
LentiCRISPRv2_gRNA2_hATG5
LentiCRISPRv2_gRNA3_hATG5
LentiCRISPRv2 (control)

d) Viral infection of the cells

Freshly produced lentiviruses were added to semi-confluent H1299 cells (seeded in 6-well plate at 10'0000 cells per well the previous day) in the presence of 8 μg/mL polybrene. After a 6-hour incubation, medium was changed to regular complete growth medium (RPMI), followed by 3 weeks of antibiotic selection with appropriate puromycin concentration.

3.5 Preparing cell lysate

After appropriate incubation period (after certain puromycin selection period or after 30 min incubation in starvation conditions), the cells are harvested from the cell culture plate following the procedure for cell passaging. Resuspended cells are transferred to a 15 mL falcon tube. They are centrifuged at 1400 rpm for 5 min. After centrifugation cells are put on ice and the supernatant is removed. To each cell pellet, 500 ul of cold PBS with protease inhibitor cocktail (in the ratio of 1:1000) is added. Cell pellet is resuspended by pipetting up and down and cells are transferred into pre-labeled Eppendorf tubes. Cells are washed once by centrifugation at 1400 rpm for 5 min and the supernatant carefully removed without disturbing the cell pellet. Depending on the size of the pellet, appropriate amount of lysis buffer is added (20 to 60 μL). Lysis buffer is freshly prepared by mixing PMSF (0.4 mM) and protease inhibitor cocktail (in the ratio of 1:1000) right before using it.

Pipetting and short vortexing of the resuspended cell pellet is then conducted so that homogenus suspension of the cells and lysis buffer is achieved. They are left on ice for 15 min and again shortly vortexed before centrifuged at 13 300 rpm for 10 min at 4°C. Supernatant is then transferred into new pre-labeled Eppendorf tubes and stored at -20ºC.

3.6 Measuring protein concentration

Total protein concentrations are determined using BCA protein assay kit, with SpectraMax M2 microplate reader at 540 nm.

Lysates are taken from the freezer at -20°C and put on ice to slowly thaw. For measuring protein concentration, lysate has to be diluted 1:10 in distilled water in order to avoid sample being too concentrated for assay to detect it accurately. Method continues as is described in the BCA assay kit manual, in summary: 8 BSA standards are made by diluting 2 μg/μL albumin standard in distilled water. Also, working reagent is prepared by mixing reagent A and B in the ratio of 50:1.

25 μL of prepared standards and samples are pipetted into appropriate wells of a 96-well plate, each in duplicate. Then 200 μL of working reagent is added to each well. Plate is incubated for 5 min at 37°C and then processed in a SpectraMax M2 microplate reader at 540 nm. Protein concentration of a sample is determined using the standard curve obtained by prepared standards.

3.7 Western Blotting

After obtaining protein concentrations of lysates, exact volumes of lysate, distilled water, loading buffer (4x) and DTT (10x) are calculated and mixed in an Eppendorf tube. The amount of loaded protein was 30 μg per sample and loading volume 20-30 μL. Amount of proteins, volume of samples and ratio of loading buffer and DTT were always the same between samples on the same gel. To denature proteins, samples were boiled at 90°C for 5 min. After they cooled down to RT, they were centrifuged at 13 000 rpm for 3 min.

Next, chamber for electrophoresis was prepared by inserting the 12% SDS-PAGE gel and filling it with running buffer. Wells in the gel were washed with running buffer by pipetting. Equal amounts of protein were put into the wells of the gel, along with molecular weight markers. The chamber was closed and electrophoresis ran for 30 min at 80 V, followed by 1 h at 135 V, until the blue marker reached the bottom of the gel.

Meanwhile, the transfer buffer was prepared. It was cooled at 4°C together with the cassette holder, 5-6 sponges, 2 filter papers and a polyvinylidene difluoride (PVDF) membrane. The membrane was activated by methanol rinse for 1 min before putting it into transfer buffer. When electrophoresis was finished and the proteins separated, they were

transferred from the gel to the membrane. The gel was removed from the electrophoresis chamber and then the transfer stack was prepared. On the backside of the cassette holder 2-3 sponges were placed, followed by the filter paper, gel, membrane, again the filter paper and 2-3 sponges. During the stacking process, any air bubbles that may have appeared in the stack were removed.

The transfer stack was placed in electrophoresis chamber filled with transfer buffer. Transferring step lasts for 1 h at 30 V for 1 gel or 60 V for 2 gels at 4°C. After transfer, the molecular weight markers on the membrane were labeled. The membrane was then soaked in tap water for 5 min, shaking followed by 1 h in blocking buffer with shaking motions. After that, the membrane was incubated in appropriate dilution of primary antibody in blocking buffer overnight on rotor at 4°C.

The following day membrane was washed three times for 6 min with TBST and incubated with the HRP-conjugated secondary antibody in blocking buffer (1:5000) at RT for 1 h. Later it was again washed three times for 5 min with TBST.

Immunoreactivity was subsequently detected using chemiluminescent substrate (Pierce ECL Plus or Laboratory-made ECL solution);

- Pierce ECL Plus: the substrate working solution is prepared by mixing Substrate A and Substrate B from the kit in a ratio of 40:1
- Lab-made ECL

The membrane was incubated with 2 ml of working solution for 1 min at RT. Then the membrane was removed from working solution and placed in a film cassette with the protein side facing up. It was covered with transparent plastic wrap and transported to the darkroom.

The film was carefully placed on top of the membrane and exposed to the illuminating substrate corresponding to specific protein bound on the membrane. The exposure time was adjusted to achieve optimal results. Light sources other than safelight must be avoided during this time. After the exposure, film was developed with the X-Omat 2000 processor. Processed membrane was then stripped by incubation in a stripping buffer for 30 min at 50°C. After washing in TBST for 5 min, the membrane was either dried and stored or the cycle was repeated with primary antibody specific to another protein of interest.

3.8 Autophagy modulation

Cells were seeded in 6-well plates or on coverslips on the bottom of 24-well plate in complete growth medium and were left to attach, recover from stress and grow for at least 24 h in the incubator at 37°C and 5% CO_2. When they reached around 75% confluence, the media was gently removed using vacuum pump. Cells were then washed with PBS and the appropriate condition was applied in each well; either nutrient-rich environment with complete growth medium in the presence and absence of CQ (10 μM) or starvation conditions, to induce autophagy, using EBSS with and without CQ (10 μM). Plate was then incubated at 37°C with 5% CO_2. After 30 min of incubation, cells were harvested and effects were observed on protein level by western blot or IF staining method.

3.9 Immunofluorescent staining

Cells were grown in a 24-well plate on coverslips and incubated in nutrient-rich or starvation conditions as described above.

The cells were thereafter washed with 300 μL of PBS at RT for 3 min, fixed with 4% PFA for 10 min at RT and further washed with PBS twice. Membrane permeabilization was achieved by treating cells with 0.05% saponin for 5 min. Coverslips were then washed with PBS for 3 min, transferred into a ceramic plate where they are covered with acetone, the additional fixative and incubated at -20°C for 10 min.

Coverslips were transferred back in the 24-well plate and they were washed with PBS twice. The coverslips were then transferred into the humidified chamber and 60 μL of blocking solution was applied on each of them. They were incubated with blocking solution at RT for 1 h.

After the blocking step, the blocking solution was removed from the coverslips with a pipette. Primary antibodies (diluted in blocking solution) were applied to the corresponding coverslips. They were incubated at 4°C overnight.

Coverslips were transferred back in the 24-well plate where they were washed with PBS twice. After, they were transferred into the humidified chamber and were covered in 60 μL of secondary antibodies, diluted in 3.5% BSA. They were incubated at RT for 1 h. The choice of secondary antibody is dependent on the donor species of the primary antibody and the desired fluorochrome. Later the coverslips were transferred back in the 24-well

plate and washed with PBS twice, 5 min per wash. Coverslips were inverted onto a cytoslide, containing 5 µL of mounting media. When mounting media was dried, the coverslips were sealed with nail polish and stored at 4°C until microscopy.

3.10 Confocal microscopy

A laser scanning confocal microscope LSM 700 from Zeiss was used to image the cytoslides. Images were taken under 630x magnification. For the Alexa488 dye, an Argon Laser with 488nm excitation was used together with the appropriate filter and 555 nm laser with the appropriate filter was used to excite the Alexa555 dye. Microscope was adjusted and images were captured with the help of Zeiss Zen software. Images were taken with the exact same settings of laser intensity, pinhole, detector gain and detector offset.

3.11 Growth curve

10'000 cells per well of H1299 *ATG5* knockout cells and H1299 control cell line were seeded in parallel in 24-well plates and incubated at 37°C with 5% CO_2. Normal complete growth medium was used. Every day for 8 days, a well of cells per cell line was detached and counted three times as described in previous sections. For cells growing for longer periods, fresh complete growth medium was provided every 3 days.

4 RESULTS AND DISCUSSION

4.1 Puromycin titration

Because we were using a new batch of puromycin and literature search for appropriate concentration of puromycin for selection of H1299 cells indicated variations from 1 to 2,5 μg/mL (68-70), we established the cell death curve and determined the appropriate concentration. For optimal selection of H1299 cells that carry pac gene, which encodes puromycin N-acetyl-transferase, we determined the lowest concentration of puromycin that killed 100% of the nonresistant (cells not carrying pac gene) wild-type cells after 8 days of selection pressure.

Cells were visually inspected daily under light microscope for any signs of cell death and/or morphological changes. H1299 is adherent cell line, so detachment of the cells is an easy detectable sign of cell death. Rounding of the cell is an indicator of its detachment. Lysed cells eventually burst, resulting in fragmentation. We took photos of the cells in culture with Zeiss axiovert-35 inverted microscope, after 4 and 8 days of selection pressure in different concentrations of puromycin. At days 4 and 8, we also detached the cells and counted the live ones based on exclusion of trypan blue positive (dead) cells.

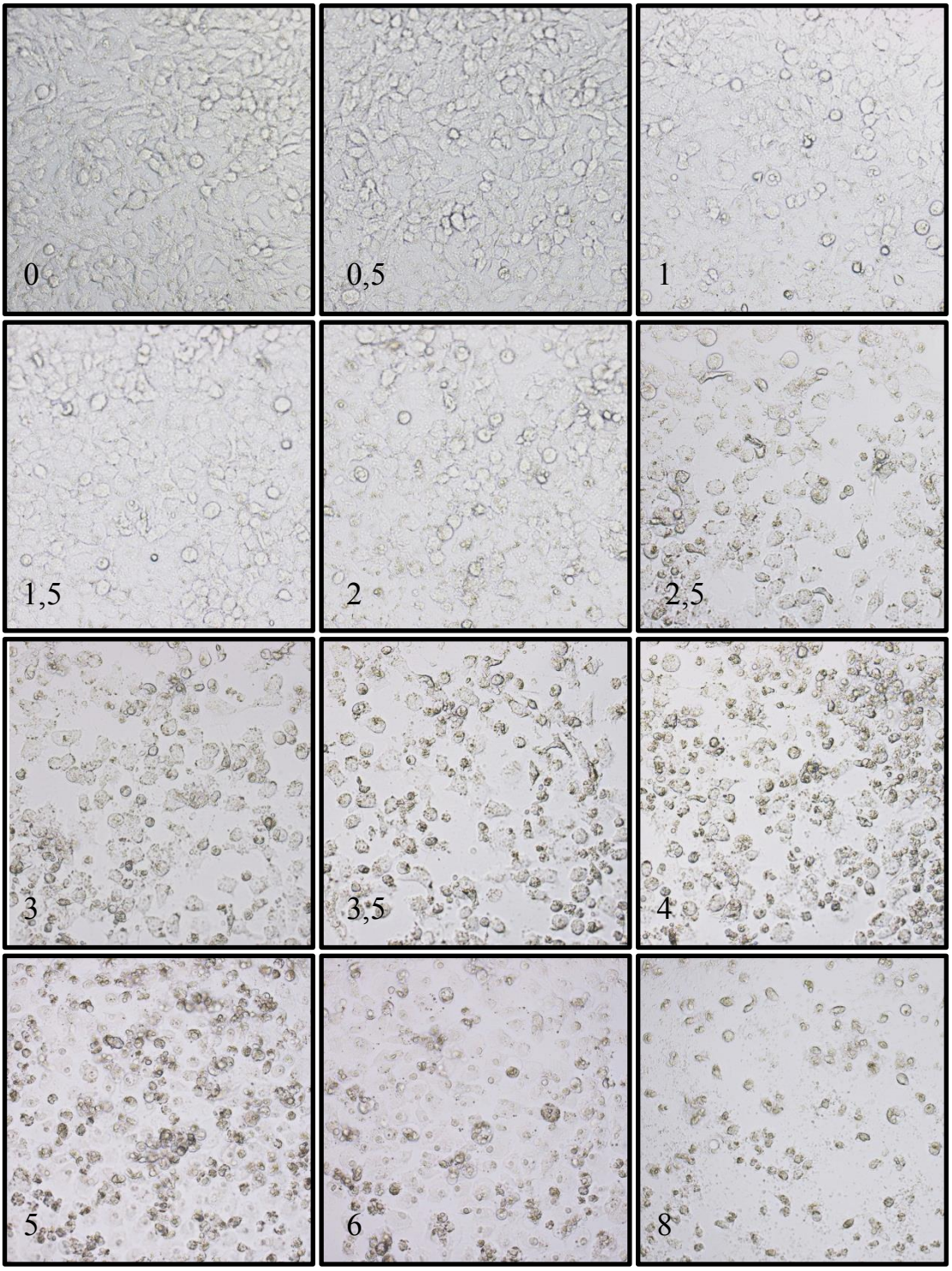

Figure 5: Appearance of wild-type H1299 cells in culture, after 4 days exposure to different concentrations of puromycin.

Cells were photographed with Zeiss Axiovert 35 microscope under 630x magnification. Numbers in the left corners of each picture indicate the concentration of puromycin [µg/mL].

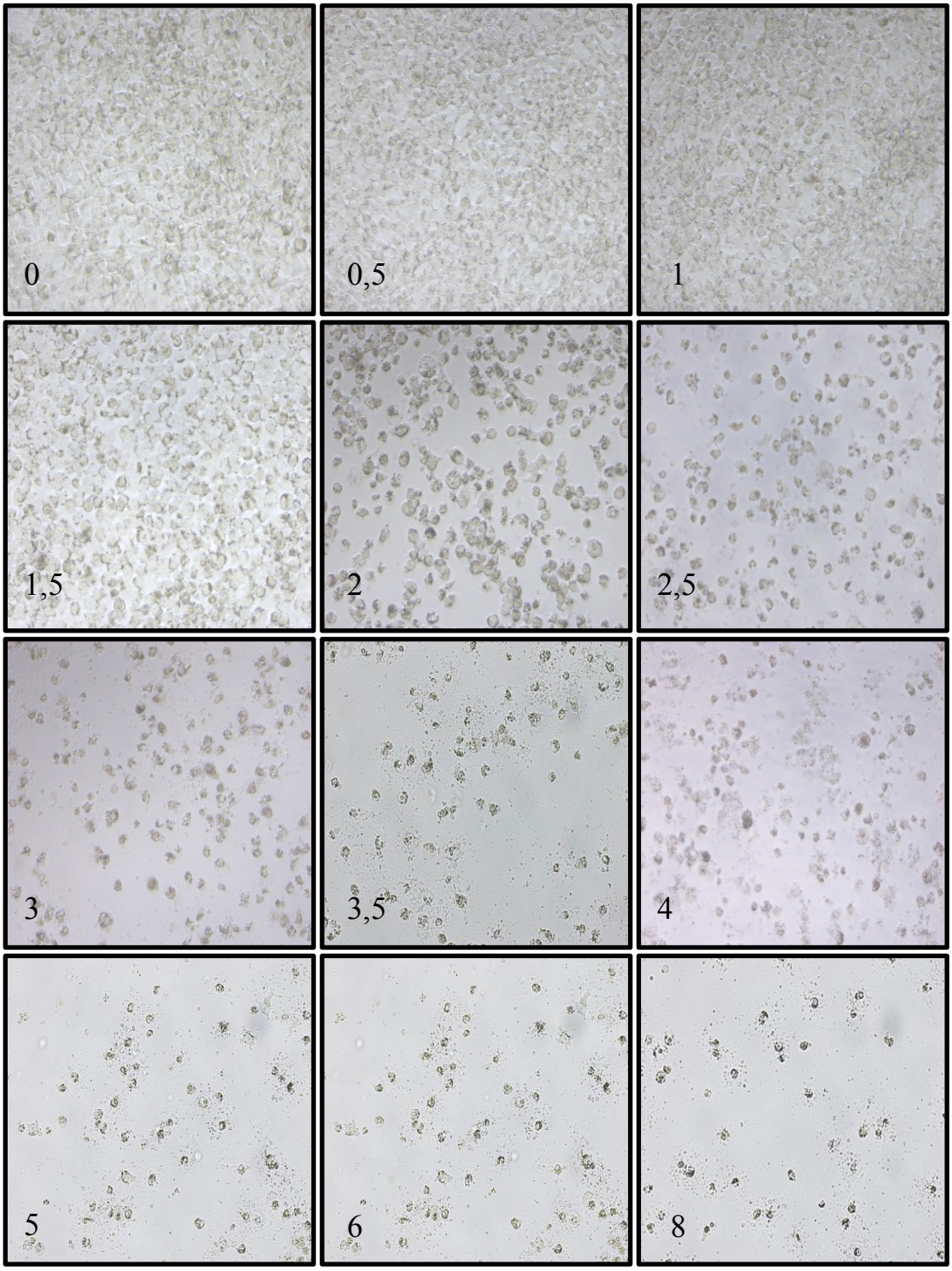

Figure 6: Appearance of wild-type H1299 cells in culture, after 8 days exposure to different concentrations of puromycin.

Cells were photographed with Zeiss Axiovert 35 microscope under 400x magnification. Numbers in the left corners of each picture indicate the concentration of puromycin [µg/mL].

A)

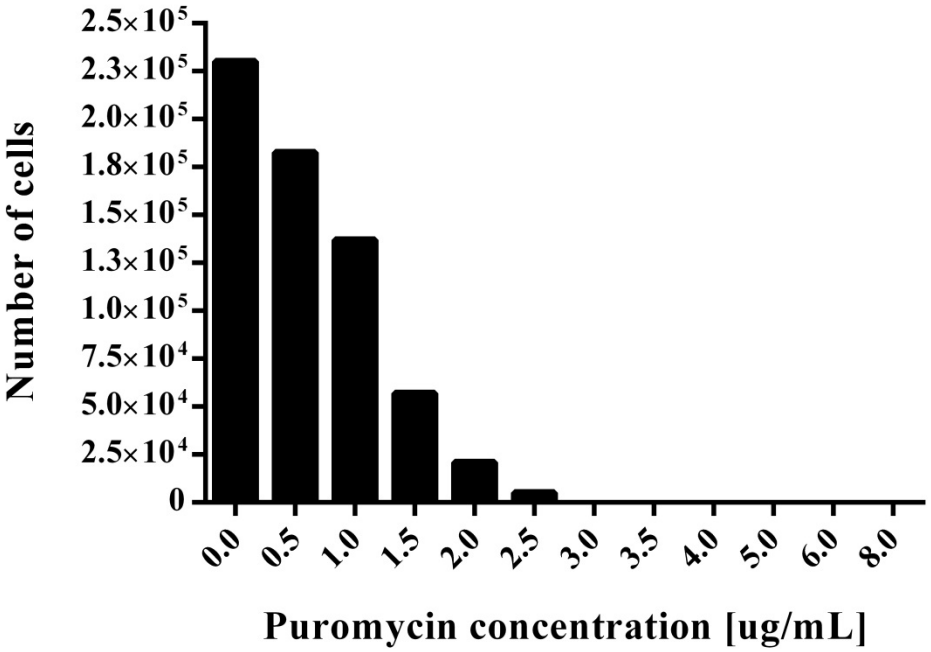

B)

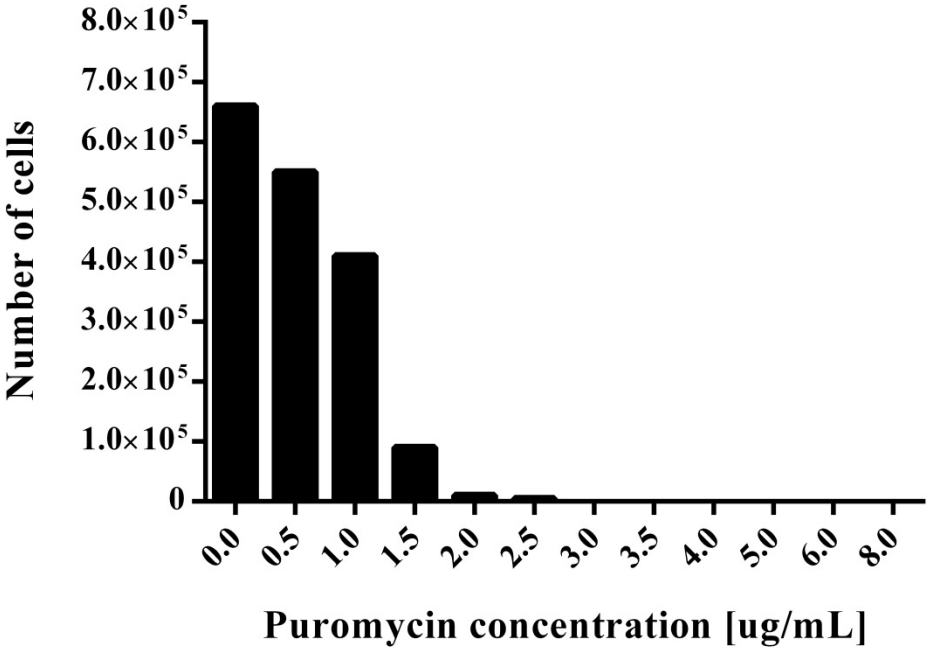

Figure 7: Number of viable wild-type H1299 cells after 4 and 8 days of selection pressure with puromycin.

Cells were detached, resuspended in 0,4% trypan blue solution and viable cells were counted after (A) 4 and (B) 8 days exposure to puromycin.

Lowest puromycin concentration of 0.5 μg/mL did not cause any significant signs of increased cell death after daily visual inspection under microscope, although cell counts revealed a slightly lower number of viable cells compared to cells grown with no puromycin (Figure 7). At 1 μg/mL of puromycin we could already observe some detached cells (Figure 5), but after 8 days in culture, the cells were still proliferating to a point of overconfluency (Figure 6). 1.5 μg/mL was the concentration that still enabled the cells to proliferate, albeit to a much lesser extent than in the control conditions with no puromycin, while at 2 μg/mL and higher cell death was much more evident and could be observed in the form of lysed and fragmented cells.

Cells exposed to 2.5 μg/mL of puromycin and higher never exceed the initial number of seeded cells (Figure 7). Concentrations of puromycin above 4 μg/mL had immediate impact on the cells and resulted in 100% cell death after just 4 days (Figure 7 A). The minimal puromycin concentration that was lethal for all the cells after 8 days exposure was 3 μg/mL.

4.2 gRNA3 exhibited successful knockout of *ATG5*

After the viral transfection of H1299 cells, we cultured them in selective medium (3 μg/mL puromycin) for 8 days before we first checked whether the knockout of the *ATG5* was successful. At that time cells were proliferating at a usual fast rate, with no visual clue for dying cells, suggesting only successfully transfected ones, carrying puromycin resistance gene were still in culture. Approximately two thirds of the cells from each viral infection were lysed and analyzed for protein expression by western blotting and a third was still left in culture in selective medium. We repeated this procedure after 2 and 3 weeks post viral transfection.

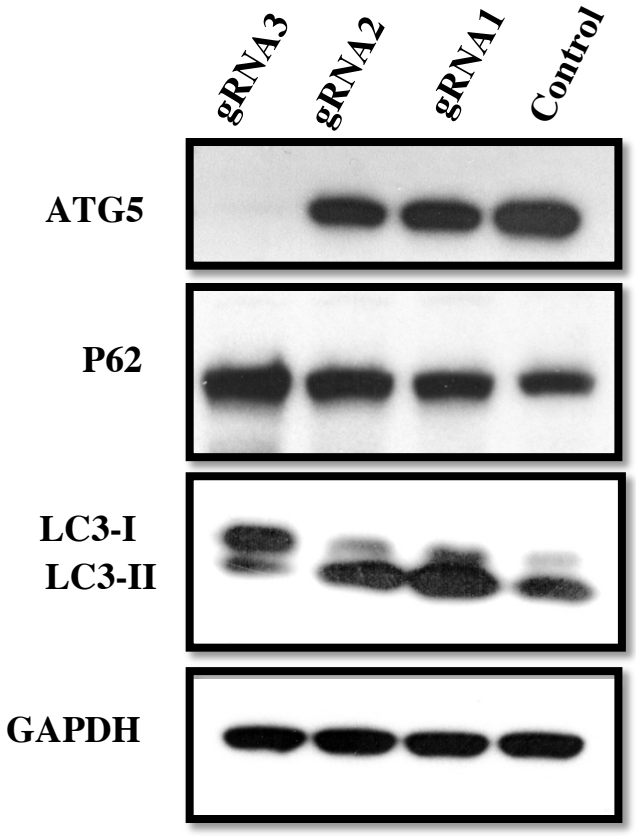

Figure 8: Validation of *ATG5* knockout cell lines by immunobloting.

Cells were kept in a selective media after the viral delivery of modified lentiCRISPRv2 plasmid. Cell lysates were collected and 30 µg of protein samples were separated with SDS-PAGE, transferred onto PVDF membrane and blotted with mouse anti-ATG5 (1:1000), rabbit anti-LC3 (1:1000), rabbit anti-P62 (1:5000) and mouse anti-GAPDH (1:10000) antibodies. Secondary anti-mouse or anti-rabbit antibodies conjugated with horseradish peroxidase (HRP) (1:5000) were added and film was developed detecting any potential chemiluminescent signal after incubation with ECL substrate. GAPDH serves as a loading control. Cell lysates were obtained in three subsequent weeks after the viral infection of the cells and three separate Western blots were made. Results shown are representative for three separate experiments.

There was little or no ATG5 protein expression in the cells targeted with CRISPR/Cas9 construct guided by gRNA3 (Figure 8). Guide RNAs 1 and 2 showed only a slight decrease in expression of ATG5 compared to control.

We also checked how lack of ATG5 expression translates to the autophagic activity of the cells by detecting the expression of LC3-I, LC3-II and P62 proteins. Western blot analysis (Figure 8) indicated there was an increase in P62 protein expression when comparing cells targeted with gRNA3 to control cell line. gRNAs 1 and 2 exhibited only a slight increase in P62 expression compared to control. Cells targeted with gRNA3 had higher expression of LC3-I and much lower expression of LC3-II compared to control.

Of the three guide RNAs used to target ATG5 genomic locus of H1299 cell line, only gRNA3 evoked successful knockout of the *ATG5*, evident by lack of protein expression. The other two CRISPR/Cas9 constructs guided by gRNA1 or gRNA2 resulted only in a minor decrease in ATG5 protein expression. Unsuccessful deletion of *ATG5* may be attributed to the lack of Cas9 expression in the cells or more likely to the possibilities that NHEJ did not result in loss-of-function mutation or only a single allele mutation occurred and cells were heterozygous, still expressing ATG5.

ATG5 is essential for autophagosome formation, which are the hallmark of autophagy. Lack of ATG5 protein expression therefore disrupts autophagic activity, although very low levels of ATG5 are sufficient for basal levels of autophagy (71). Therefore, only a successful knockout of *ATG5* sufficiently disables autophagy.

P62 is a specific substrate for autophagy degradation, so there is inverse correlation between total expression levels of P62 and autophagic activity (37). Cytosolic LC3-I gets converted in LC3-II in autophagic process and LC3-II is present on autophagosomes (57). Taken together results from Figure 8, indicate disrupted autophagy in gRNA3-targeted cells, although further assessment is needed

4.3 H1299 *ATG5* KO cells are deficient in autophagy

To confirm absence of autophagy in *ATG5* KO cells (gRNA3), we exposed the cells to starvation conditions, which would normally induce autophagy and compare them with Control cell line. EBSS, the amino acid deficient medium was used for this purpose. Controls with CQ were also used. We detected the effects by immunoblot analysis, where we checked the expression of ATG5, P62, LC3-I and LC3-II and by immunofluorescence staining, detecting ATG5 and LC3.

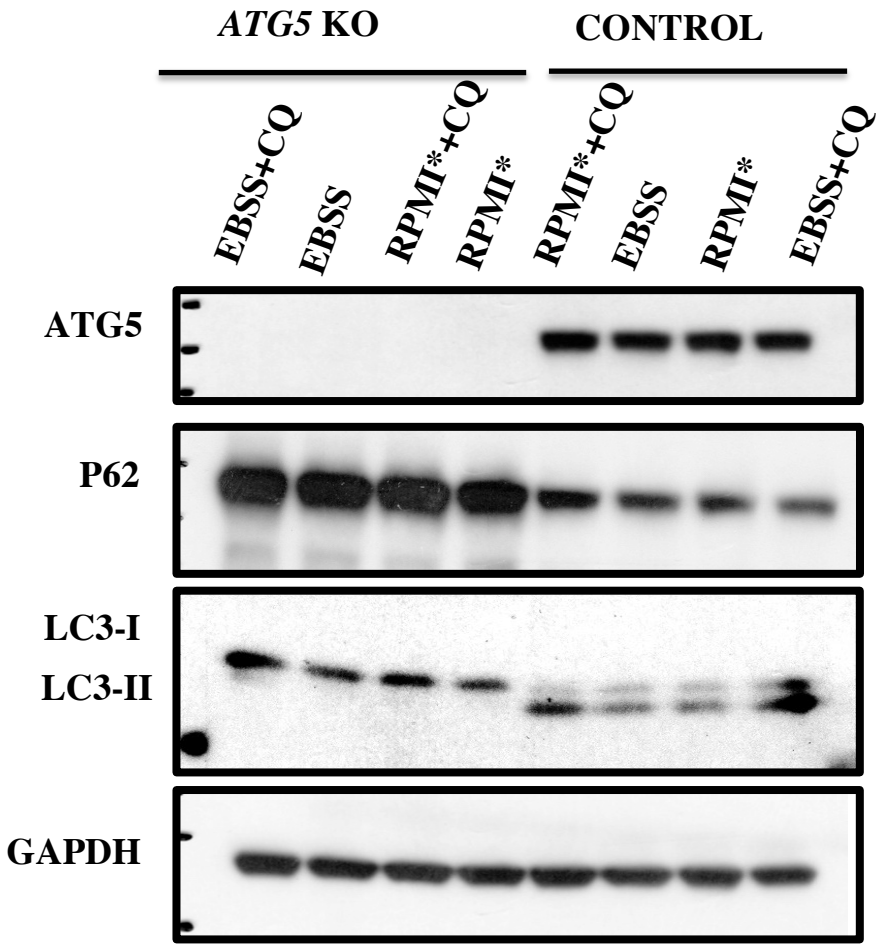

Figure 9: Autophagy induction by starvation.

H1299 *ATG5* KO cell line and H1299 control were simultaneously incubated for 30 min in growth culture under 4 different conditions: normal complete growth medium (RPMI*) and nutrient lacking medium (EBSS) both with and without CQ (10 μM). After 30 min cells were collected, lysed and 30 μg of lysate per sample was analyzed with western blot. Specific antibodies used were: mouse anti-ATG5 (1:1000), rabbit anti-LC3 (1:1000), rabbit anti-P62 (1:5000). Mouse anti-GAPDH (1:10000) served as a loading control.

Western blot analysis (Figure 9) showed no expression of ATG5 in H1299 *ATG5* KO cells, while control cell line had stable expression of ATG5 in all of the experimental settings. *ATG5* KO cells had stable expression of P62 regardless if the cells had been exposed to normal conditions, autophagy inducing conditions and/or inhibitor of late stage of autophagy (CQ) and it was notably higher compared to control cell line. P62 expression slightly varied between different conditions in Control cell line: it was the highest in cells incubated in normal complete growth medium (RPMI*) with CQ treatment, followed by RPMI*, EBSS and the least expression of P62 was observed in control cells incubated in EBSS with CQ.

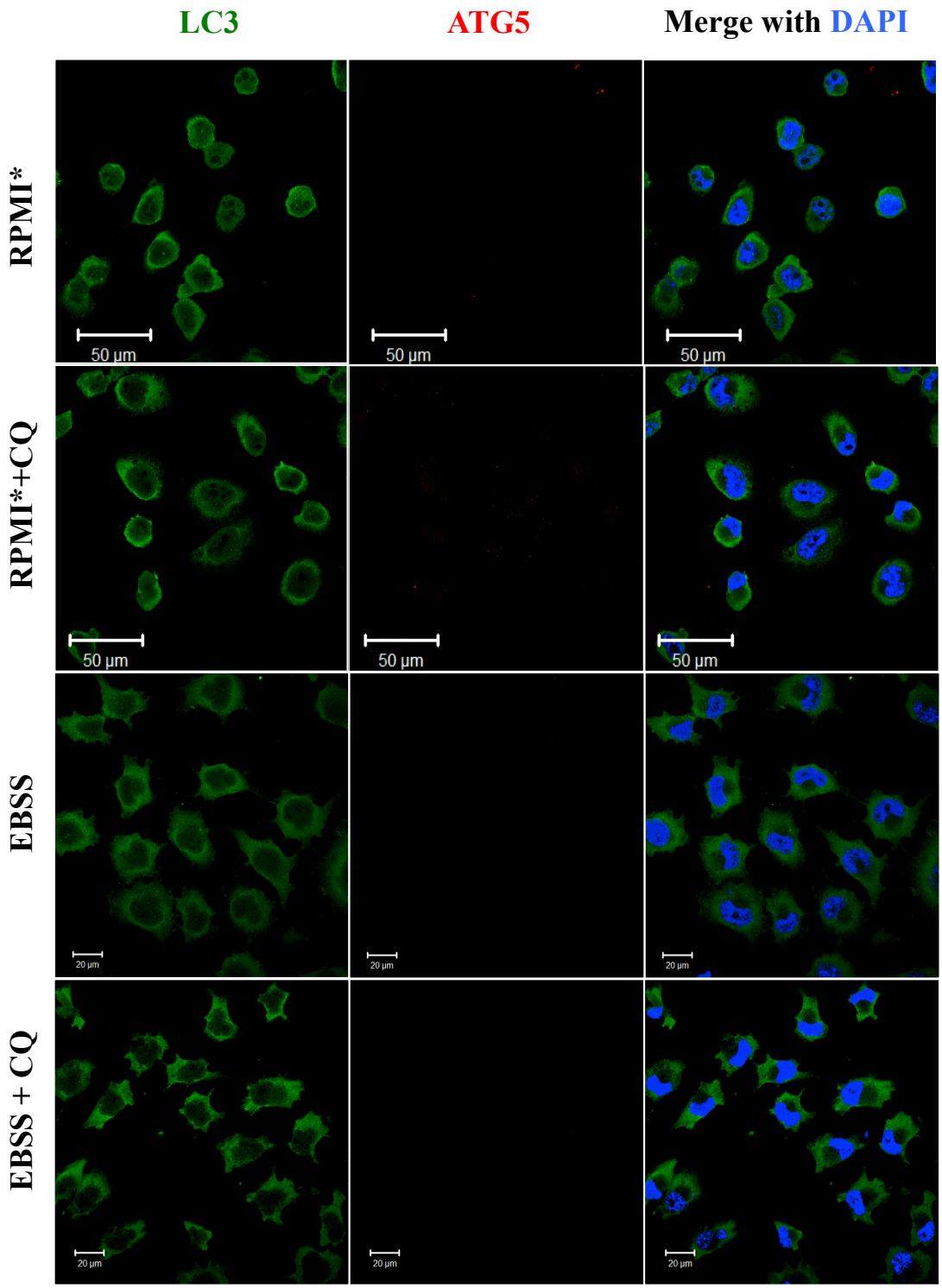

Figure 10: H1299 *ATG5* KO cells are unable to form autophagosomes.

H1299 *ATG5* KO cells were seeded on coverlips and incubated in complete growth medium at 37ºC and 5% CO_2. The next day they were rinsed in PBS and incubated in different conditions for 30min at 37ºC and 5% CO_2: complete growth medium (RPMI*), complete growth medium with 10uM CQ (RPMI*+CQ), EBSS or EBSS with 10uM CQ (EBSS+CQ). After 30min, immunofluorescent staining was performed with rabbit-anti-human LC3 (1:100) and mouse-anti-human ATG5 (1:100) primary antibodies followed by addition of goat-anti-rabbit 488 (1:400) and goat-anti-mouse 555 (1:400) secondary antibodies. Stained cytoslides were photographed with ZEISS LSM 700 confocal microscope under 630x magnification. Scale: 50 µm for RPMI* and RPMI*+CQ, 20 µm for EBSS and EBSS+CQ.

ATG5 KO cells had no expression of LC3-II, but stable and higher than control cell line expression of LC3-I (Figure 9). There was no change in LC3-II expression evident between starvation and control conditions in control cell line if no CQ treatment had been applied, while LC3-II expression was increased if late stage of autophagy had been inhibited by CQ, the most if cells had been incubated in EBSS.

Immunofluorescent staining of ATG5 and LC3 proteins in *ATG5* KO cells (Figure 10) gave similar results to western blot analysis. The cells stained negative for ATG5 expression, which confirmed a successful knockout of *ATG5.* There was a diffuse green fluorescence throughout the cytoplasm with no evident puncta, indicating there was no conversion of LC3-I to LC3-II, which would be seen as green puncta representing autophagosomes. No difference in staining between different conditions could be observed in H1299 KO cells.

There was however, a change in *ATG5* KO cells morphology (Figure 10), where the cells exposed to normal complete growth medium appeared to be more rounded, while cells exposed to starvation conditions had more dendritic-like morphology, especially in the case of simultaneous treatment with CQ and EBSS.

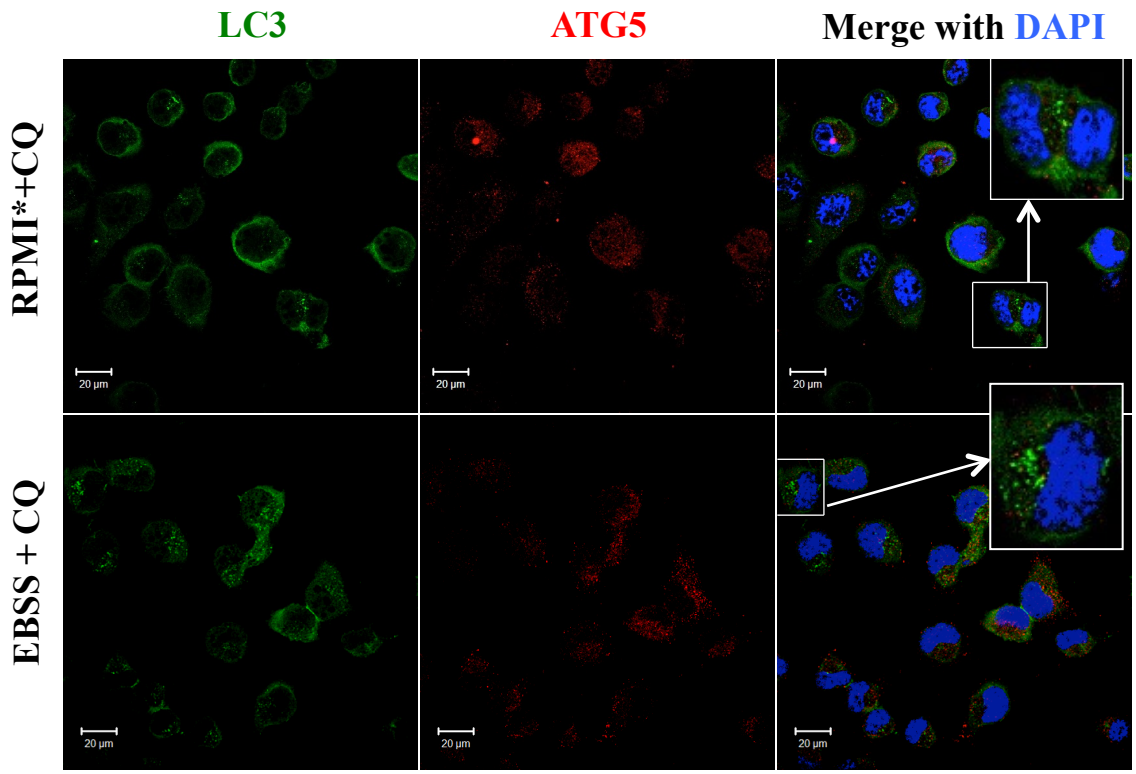

Figure 11: H1299 control cell line increased formation of autophagosomes under autophagy induction.

H1299 control cell line was treated the same as *ATG5* KO cells in (Figure 10). Stained cytoslides were photographed with ZEISS LSM 700 confocal microscope under 630x magnification. Scale: 20 µm

The H1299 control cell line stained positive for ATG5 expression (Figure 11). LC3 staining revealed only a few green puncta in cells in control conditions (RPMI* + 10 µM CQ) and increased number of green punctate structures in starvation conditions (EBSS + 10 µM CQ). Interestingly there was no change in morphology of the cells when comparing cells exposed to starvation and control conditions.

Basal autophagy of H1299 control cell line was induced under starvation conditions indicated by decreased amount of P62 and increased autophagosome formation. The amount of LC3-II remained similar in the control cell line even under autophagy-inducing starvation conditions when CQ treatment had not been applied and was only increased when lysosomal degradation had been partially prevented by CQ. This is consistent with report where degradation of LC3-II is proportionally increased together with autophagic flux, which is attributed to high degradation capacity (60).

Taken together, we can confirm the lack of autophagy in *ATG5* KO cells, which were not

able to sustain even the basal levels of autophagy, much less induced; expected result consistent with loss of ATG5 function. Control cell line on the other hand had unrestricted autophagy and cells which otherwise have low levels of autophagy responded to starvation with increased autophagic activity.

4.4 H1299 *ATG5* KO cells have higher growth rate than the control

We wanted to see if there is any effect of *ATG5* knockout on the growth rate of the cells, so we compared growth rates of the H1299 *ATG5* KO and the H1299 control cell line. We seeded both cell lines in parallel and counted them daily for 8 days.

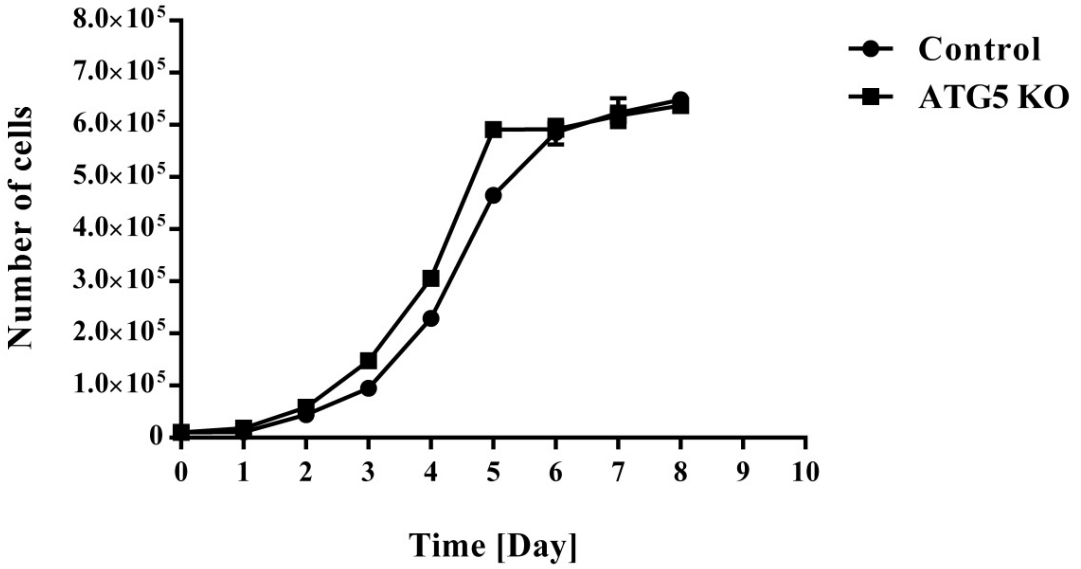

Figure 12: Growth curves of H1299 *ATG5* KO and control cell lines.

10000 cells of H1299 *ATG5* KO and control were seeded in parallel in a 24-well plate in optimal growth medium and incubated at 37°C and 5% CO_2. New wells of cells were detached and counted daily for 8 days. At day 3 and 6 new fresh growth medium was provided for the cells still in culture. Individual values are plotted as mean of three counts with standard deviation.

Both growth curves (Figure 12) were sigmoid shape, with lower and upper asymptotes. Lower asymptote was fixed at 10000 (number of cells seeded) and upper asymptote was set at $6{,}6 \times 10^{\wedge -5}$ (arbitrarily defined number reflecting maximal number of H1299 cells on 2 cm^2 surface in 24-well cell culture plate).

Using nonlinear regression, we fitted Logistic, Gompertz, and Weibull growth models (Table VIII) in GraphPad Prism software. With extra sum of squares F test we, compared the goodness of fit of two alternative nested models at a time.

Weibull growth model fitted significantly better than Gompertz growth model to both H1299 *ATG5* KO ($F_{1, 24} = 176.3$, $p < .0001$, $\alpha = 0.05$) and H1299 control cell line ($F_{1, 24} = 574.8$, $p < .0001$, $\alpha = 0.05$) growth pattern.

Weibull growth model fitted significantly better than logistic growth model to both H1299 *ATG5* KO ($F_{1, 24} = 28.03$, $p < .0001$, $\alpha = 0.05$) and H1299 control cell line ($F_{1, 24} = 75.75$, $p < .0001$, $\alpha = 0.05$) growth pattern.

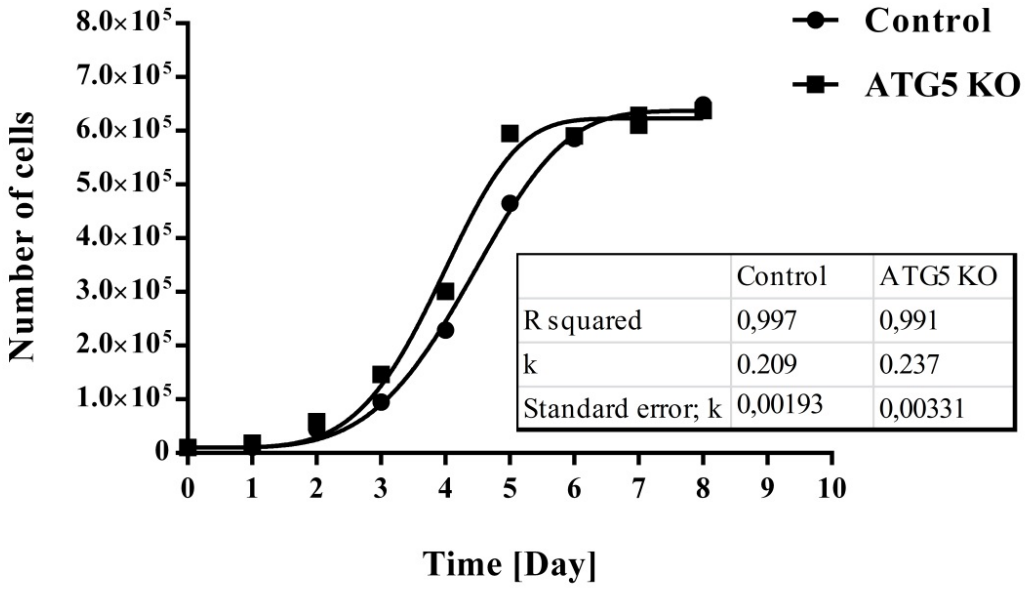

	Control	ATG5 KO
R squared	0,997	0,991
k	0.209	0.237
Standard error; k	0,00193	0,00331

Figure 13: Weibull growth model was fitted to growth curves of H1299 *ATG5* KO and H1299 control cell line.

Weibull growth model was fitted with GraphPad Prism 6.0 software, based on Weibull growth model equation (Table VIII).

With extra sum of squares F-test, we then tested if a single curve fitted to Weibull growth model could adequately fit all the data sets. The null hypothesis that parameters k, g and Ymax are the same for all data sets was rejected, so separate curves described the data sets better ($F_{3, 48} = 24.12$, $p < .0001$, $\alpha = 0.03$).

The same statistic method was used for determining if the growth rates (k) were the same for both growth curves fitted to Weibull growth model. Growth rates were significantly different between H1299 *ATG5* KO and the H1299 control cell line ($F_{1, 48} = 52.54$, $p < .0001$, $\alpha = 0.05$).

Table VIII: Growth models

Growth model equations	Parameters
• Gompertz; Y=Ymax×exp(ln(Y0/Ymax) × exp(-k× x))	• Ymax; upper asimptote • Y0; lower asimptote • k; growth rate • g; a parameter that controls the x-ordinate for the point of inflection
• Logistic; Y=Ymax×Y0/(Ymax-Y0)×exp(-k×x)+Y0)	
• Weibull; Y=Ymax-(Ymax-Y0) × exp(-1× ((k×x)^g)	

Our observation that *ATG5* KO cells proliferate faster than cells with unrestricted ATG5 expression is in line with previous work of Liu et al (72) where they showed that in an in vitro model of melanoma down regulation of ATG5 resulted in increased proliferation. It was also reported that enforced expression of ATG5 reduced tumor growth (63) and similarly enforced expression of another crucial ATG protein, beclin 1, slowed the proliferation of tumor cell lines (73). Furthermore, ATG5-deficient hepatocytes were shown to have growth advantage over normal cell counterparts (44). In contrast, there are also reports of inhibited proliferation of cells lacking ATG5 expression. Mammalian pulmonary artery cells with *ATG5* knockdown for example, had slower proliferation rate than wild-type cells (74). This indicates that the effect of autophagy on growth rates might be cell type and /or cell state dependent.

H1299 is human non-small lung cancer cell line that has homozygous mutation of TP53 gene, thus lacking the expression of p53 protein. p53 is a known tumor suppressor, exerting its function by transducing signals of stressful stimuli, resulting in a series of anti-proliferative responses. One such major response is apoptosis (75). When blocking autophagy in cells in vitro that have disabled apoptotic machinery, researchers reported decreased cell death, explained by disabling cells to undergo alternative autophagic cell death, a process directed by ATG5 and beclin 1 (76). Similar settings may explain the difference in cell growth between H1299 *ATG5* KO and the control cell line. Although in our case apoptotic machinery was not disabled in H1299 cells, apoptosis is partially hindered due to lack of p53 expression and simultaneous blocked autophagy in *ATG5* KO

cells may result in increased cell growth in comparison to the control cell line. Perhaps further experiments could be conducted to test this theory, such as similar analysis of additional *beclin 1* knockout in H1299 cells.

Another theory that could explain the difference in cell growth perhaps lies in the reported inverse correlation between rates of autophagy and cell growth. Stressful conditions that stimulate autophagy, such as starvation, overconfluent cell culture, rapamycin treatment, may reduce the rate of cell growth (although the mechanisms behind it may differ) (77). Overconfluency was present in our experimental settings in latter stages and it might have contributed to inducing autophagy in autophagy competent control cells. We could test this theory with similar growth rate experiment, but with additional rapamycin treatment of both cell lines and observe if even bigger difference in growth rates arises.

5 CONCLUSION

Autophagy has been extensively studied in the past decades evidenced by steady increase in number of scientific papers on autophagy published each year, from 599 published in 2007 to 4736 published in 2016 (according to PubMed). Even tough 2016 Nobel Prize in physiology or medicine was awarded to Yoshinori Ohsumi for his role in discovering and elucidating the mechanisms underlying autophagy, much is still to be uncovered in this field, especially the exact role and affiliations of autophagy in pathological pathways in human.

In this master thesis, we successfully established *ATG5* knockout from H1299 cell line using CRISPR/Cas9 genome editing technology, which proved to be a powerful tool for genome modification that allows for fast and efficient establishment of experimental models. Although we demonstrated successful *ATG5* knockout by indirect methods, detecting the expression of protein encoded by the gene, we could use a direct approach, amplifying the target region and conduct mismatch cleavage assay to detect indels. We would also suggest characterization of possible off-target effects with next generation sequencing. H1299 *ATG5* KO cells were unable to perform autophagy even in basal conditions in contrast to the control cell line. *ATG5* knockout affected cell growth, which was accelerated in cells lacking ATG5 expression. These data suggest that autophagy inhibition or *ATG5* ablation could negatively affect the effort of tumor growth suppression in non-small cell lung cancer. Of course this might not translate to in vivo conditions, so further studies should be made to confirm it. Considering other publications in autophagy research field, our findings add some new insights on a scale of autophagy having diverse implications in pathophysiological pathways, depending on cell type and circumstances.

In conclusion, our work represents a small piece in mosaic of research that is trying to elucidate the role of autophagy in the context of cancer. The use of innovative new techniques for genome engineering may facilitate a faster path towards achieving this goal.

6 REFERENCES

1 Brouns SJJ, Jore MM, Lundgren M, et al. Small CRISPR RNAs guide antiviral defense in prokaryotes. Science 2008; 321 (5891): 960-964.

2 Doudna JA, Charpentier E. The new frontier of genome engineering with CRISPR-Cas9. Science 2014; 346 (6213): 1258096.

3 Hsu PD, Scott DA, Weinstein JA, et al. DNA targeting specificity of RNA-guided Cas9 nucleases. Nature biotechnology 2013; 31 (9): 827-832.

4 Jinek M, Chylinski K, Fonfara I, et al. A programmable dual-RNA–guided DNA endonuclease in adaptive bacterial immunity. Science 2012; 337 (6096): 816-821.

5 Ran FA, Hsu PD, Wright J, et al. Genome engineering using the CRISPR-Cas9 system. Nature protocols 2013; 8 (11): 2281-2308.

6 Ishino Y, Shinagawa H, Makino K, et al. Nucleotide sequence of the iap gene, responsible for alkaline phosphatase isozyme conversion in Escherichia coli, and identification of the gene product. Journal of bacteriology 1987; 169 (12): 5429-5433.

7 Mojica FJM, Díez‐Villaseñor C, Soria E, et al. Biological significance of a family of regularly spaced repeats in the genomes of Archaea, Bacteria and mitochondria. Molecular microbiology 2000; 36 (1): 244-246.

8 Grissa I, Vergnaud G, Pourcel C. The CRISPRdb database and tools to display CRISPRs and to generate dictionaries of spacers and repeats. BMC bioinformatics 2007; 8 (1): 172.

9 Jansen R, Embden J, Gaastra W, et al. Identification of genes that are associated with DNA repeats in prokaryotes. Molecular microbiology 2002; 43 (6): 1565-1575.

10 Bolotin A, Quinquis B, Sorokin A, et al. Clustered regularly interspaced short palindrome repeats (CRISPRs) have spacers of extrachromosomal origin. Microbiology 2005; 151 (8): 2551-2561.

11 Mojica FJM, García-Martínez J, Soria E. Intervening sequences of regularly spaced prokaryotic repeats derive from foreign genetic elements. Journal of molecular evolution 2005; 60 (2): 174-182.

12 Barrangou R, Fremaux C, Deveau H, et al. CRISPR provides acquired resistance against viruses in prokaryotes. Science 2007; 315 (5819): 1709-1712.

13 Barrangou R, Horvath P. CRISPR: new horizons in phage resistance and strain identification. Annual review of food science and technology 2012; 3: 143-162.

14 Marraffini LA, Sontheimer EJ. CRISPR interference limits horizontal gene transfer in staphylococci by targeting DNA. science 2008; 322 (5909): 1843-1845.

15 Abudayyeh OO, Gootenberg JS, Konermann S, et al. C2c2 is a single-component programmable RNA-guided RNA-targeting CRISPR effector. Science 2016: aaf5573.

16 Ran FA, Hsu PD, Lin C-Y, et al. Double nicking by RNA-guided CRISPR Cas9 for enhanced genome editing specificity. Cell 2013; 154 (6): 1380-1389.

17 Fu Y, Sander JD, Reyon D, et al. Improving CRISPR-Cas nuclease specificity using truncated guide RNAs. Nature biotechnology 2014; 32 (3): 279-284.

18 Pardo B, Gómez-González B, Aguilera A. DNA repair in mammalian cells. Cellular and Molecular Life Sciences 2009; 66 (6): 1039-1056.

19 Choi PS, Meyerson M. Targeted genomic rearrangements using CRISPR/Cas

technology. Nature communications 2014; 5.
20 Liu ET, Bolcun‐Filas E, Grass DS, et al. Of mice and CRISPR. EMBO reports 2017: e201643717.
21 Chen B, Gilbert LA, Cimini BA, et al. Dynamic imaging of genomic loci in living human cells by an optimized CRISPR/Cas system. Cell 2013; 155 (7): 1479-1491.
22 Shalem O, Sanjana NE, Hartenian E, et al. Genome-scale CRISPR-Cas9 knockout screening in human cells. Science 2014; 343 (6166): 84-87.
23 Cyranoski D. CRISPR gene-editing tested in a person for the first time. Nature News 2016; 539 (7630): 479.
24 Evitt NH, Mascharak S, Altman RB. Human germline CRISPR-Cas modification: toward a regulatory framework. The American Journal of Bioethics 2015; 15 (12): 25-29.
25 Ohsumi Y. Historical landmarks of autophagy research. Cell research 2014; 24 (1): 9-23.
26 Liu H, He Z, Simon H-U. Protective role of autophagy and autophagy-related protein 5 in early tumorigenesis. Journal of molecular medicine 2015; 93 (2): 159-164.
27 Shintani T, Klionsky DJ. Autophagy in health and disease: a double-edged sword. Science 2004; 306 (5698): 990-995.
28 Liu H, He Z, Simon H-U. Targeting autophagy as a potential therapeutic approach for melanoma therapy. Seminars in cancer biology: Elsevier, 2013:352-360.
29 Galluzzi L, Pietrocola F, Bravo‐San Pedro JM, et al. Autophagy in malignant transformation and cancer progression. The EMBO journal 2015; 34 (7): 856-880.
30 Mizushima N, Levine B, Cuervo AM, et al. Autophagy fights disease through cellular self-digestion. Nature 2008; 451 (7182): 1069-1075.
31 Mizushima N. The pleiotropic role of autophagy: from protein metabolism to bactericide. Cell Death & Differentiation 2005; 12: 1535-1541.
32 Rao S, Tortola L, Perlot T, et al. A dual role for autophagy in a murine model of lung cancer. Nature communications 2014; 5.
33 Hayat MA. Autophagy: Cancer, Other Pathologies, Inflammation, Immunity, Infection, and Aging: Volume 8- Human Diseases. Elsevier Science, 2015.
34 Yang Z, Klionsky DJ. Mammalian autophagy: core molecular machinery and signaling regulation. Current opinion in cell biology 2010; 22 (2): 124-131.
35 Lamb CA, Yoshimori T, Tooze SA. The autophagosome: origins unknown, biogenesis complex. Nature reviews Molecular cell biology 2013; 14 (12): 759-774.
36 Yang Y-p, Liang Z-q, Gu Z-l, et al. Molecular mechanism and regulation of autophagy. Acta Pharmacologica Sinica 2005; 26 (12): 1421-1434.
37 Mizushima N, Yoshimori T, Levine B. Methods in mammalian autophagy research. Cell 2010; 140 (3): 313-326.
38 Laplante M, Sabatini DM. Regulation of mTORC1 and its impact on gene expression at a glance. The Company of Biologists Ltd, 2013.
39 Glick D, Barth S, Macleod KF. Autophagy: cellular and molecular mechanisms. The Journal of pathology 2010; 221 (1): 3-12.
40 Ohsumi Y. Molecular dissection of autophagy: two ubiquitin-like systems. Nature reviews Molecular cell biology 2001; 2 (3): 211-216.
41 He C, Klionsky DJ. Regulation mechanisms and signaling pathways of autophagy. Annual review of genetics 2009; 43: 67-93.
42 Qu X, Yu J, Bhagat G, et al. Promotion of tumorigenesis by heterozygous

disruption of the beclin 1 autophagy gene. The Journal of clinical investigation 2003; 112 (12): 1809-1820.
43 Kuma A, Hatano M, Matsui M, et al. The role of autophagy during the early neonatal starvation period. Nature 2004; 432 (7020): 1032-1036.
44 Takamura A, Komatsu M, Hara T, et al. Autophagy-deficient mice develop multiple liver tumors. Genes & development 2011; 25 (8): 795-800.
45 Liu H, He Z, Simon H-U. Autophagy suppresses melanoma tumorigenesis by inducing senescence. Autophagy 2014; 10 (2): 372-373.
46 Degenhardt K, Mathew R, Beaudoin B, et al. Autophagy promotes tumor cell survival and restricts necrosis, inflammation, and tumorigenesis. Cancer cell 2006; 10 (1): 51-64.
47 Karantza-Wadsworth V, Patel S, Kravchuk O, et al. Autophagy mitigates metabolic stress and genome damage in mammary tumorigenesis. Genes & development 2007; 21 (13): 1621-1635.
48 Mathew R, Karp CM, Beaudoin B, et al. Autophagy suppresses tumorigenesis through elimination of p62. Cell 2009; 137 (6): 1062-1075.
49 Rosenfeldt MT, Ryan KM. The role of autophagy in tumour development and cancer therapy. Expert reviews in molecular medicine 2009; 11: e36.
50 Yang ZJ, Chee CE, Huang S, et al. The role of autophagy in cancer: therapeutic implications. Molecular cancer therapeutics 2011; 10 (9): 1533-1541.
51 Han W, Pan H, Chen Y, et al. EGFR tyrosine kinase inhibitors activate autophagy as a cytoprotective response in human lung cancer cells. PloS one 2011; 6 (6): e18691.
52 Ertmer A, Huber V, Gilch S, et al. The anticancer drug imatinib induces cellular autophagy. Leukemia 2007; 21 (5): 936-942.
53 Li X, Fan Z. The epidermal growth factor receptor antibody cetuximab induces autophagy in cancer cells by downregulating HIF-1α and Bcl-2 and activating the beclin 1/hVps34 complex. Cancer research 2010; 70 (14): 5942-5952.
54 Liu Y-L, Yang P-M, Shun C-T, et al. Autophagy potentiates the anti-cancer effects of the histone deacetylase inhibitors in hepatocellular carcinoma. Autophagy 2010; 6 (8): 1057-1065.
55 Sui X, Chen R, Wang Z, et al. Autophagy and chemotherapy resistance: a promising therapeutic target for cancer treatment. Cell death & disease 2013; 4 (10): e838.
56 Kimmelman AC. The dynamic nature of autophagy in cancer. Genes & development 2011; 25 (19): 1999-2010.
57 Klionsky DJ, Abdalla FC, Abeliovich H, et al. Guidelines for the use and interpretation of assays for monitoring autophagy. Autophagy 2012; 8 (4): 445-544.
58 Klionsky DJ. For the last time, it is GFP-Atg8, not Atg8-GFP (and the same goes for LC3). Autophagy 2011; 7 (10): 1093-1094.
59 Mizushima N, Yamamoto A, Matsui M, et al. In vivo analysis of autophagy in response to nutrient starvation using transgenic mice expressing a fluorescent autophagosome marker. Molecular biology of the cell 2004; 15 (3): 1101-1111.
60 Mizushima N, Yoshimori T. How to interpret LC3 immunoblotting. Autophagy 2007; 3 (6): 542-545.
61 Bjørkøy G, Lamark T, Pankiv S, et al. Monitoring autophagic degradation of p62/SQSTM1. Methods in enzymology 2009; 452: 181-197.
62 Kim M, Sandford E, Gatica D, et al. Mutation in ATG5 reduces autophagy and

leads to ataxia with developmental delay. Elife 2016; 5: e12245.
63 Yousefi S, Perozzo R, Schmid I, et al. Calpain-mediated cleavage of Atg5 switches autophagy to apoptosis. Nature cell biology 2006; 8 (10): 1124-1132.
64 Codogno P, Meijer AJ. Atg5: more than an autophagy factor. Nature cell biology 2006; 8 (10): 1045-1046.
65 Zhang lab MIT. CRISPR design. http://crispr.mit.edu. Dostopano: 24 Jun-2016.
66 Zhang lab GeCKO. LENTIVIRAL CRISPR TOOLBOX. http://genome-engineering.org/gecko/wp-content/uploads/2013/12/lentiCRISPRv2-and-lentiGuide-oligo-cloning-protocol.pdf. Dostopano: 6 Jul-2016.
67 Addgene: lentiCRISPR v2. 2017; 2017.
68 Baptiste-Okoh N, Barsotti AM, Prives C. A role for caspase 2 and PIDD in the process of p53-mediated apoptosis. Proceedings of the National Academy of Sciences 2008; 105 (6): 1937-1942.
69 Geißler V, Altmeyer S, Stein B, et al. The RNA helicase Ddx5/p68 binds to hUpf3 and enhances NMD of Ddx17/p72 and Smg5 mRNA. Nucleic acids research 2013: gkt538.
70 Nasser MW, Datta J, Nuovo G, et al. Down-regulation of micro-RNA-1 (miR-1) in lung cancer suppression of tumorigenic property of lung cancer cells and their sensitization to doxorubicin-induced apoptosis by miR-1. Journal of Biological Chemistry 2008; 283 (48): 33394-33405.
71 Hosokawa N, Hara Y, Mizushima N. Generation of cell lines with tetracycline‐regulated autophagy and a role for autophagy in controlling cell size. FEBS letters 2006; 580 (11): 2623-2629.
72 Liu H, He Z, von Rütte T, et al. Down-regulation of autophagy-related protein 5 (ATG5) contributes to the pathogenesis of early-stage cutaneous melanoma. Science translational medicine 2013; 5 (202): 202ra123-202ra123.
73 Koneri K, Goi T, Hirono Y, et al. Beclin 1 gene inhibits tumor growth in colon cancer cell lines. Anticancer research 2007; 27 (3B): 1453-1457.
74 Long L, Yang X, Southwood M, et al. Chloroquine Prevents Progression of Experimental Pulmonary Hypertension via Inhibition of Autophagy and Lysosomal Bone Morphogenetic Protein Type II Receptor DegradationNovelty and Significance. Circulation research 2013; 112 (8): 1159-1170.
75 Fridman JS, Lowe SW. Control of apoptosis by p53. Oncogene 2003; 22 (56): 9030-9040.
76 Shimizu S, Kanaseki T, Mizushima N, et al. Role of Bcl-2 family proteins in a non-apoptotic programmed cell death dependent on autophagy genes. Nature cell biology 2004; 6 (12): 1221-1228.
77 Meléndez A, Neufeld TP. The cell biology of autophagy in metazoans: a developing story. Development 2008; 135 (14): 2347-2360.